Available online at www.sciencedirect.com
SCIENCE DIRECT®
Geochimica et Cosmochimica Acta 70 (2006) 2337–2353
Geochimica
www.elsevier.com/locate/gca

The structural behavior of ferric and ferrous iron in aluminosilicate glass near meta-aluminosilicate joins

Bjorn O. Mysen *

Geophysical Laboratory, Carnegie Institution of Washington, 5251 Broad Branch Rd., NW, Washington, DC 20015, USA

Received 29 June 2005; accepted in revised form 24 January 2006

Abstract

Iron-57 resonant absorption Mössbauer spectroscopy was used to describe the redox relations and structural roles of Fe^{3+} and Fe^{2+} in meta-aluminosilicate glasses. Melts were formed at 1500 °C in equilibrium with air and quenched to glass in liquid H_2O with quenching rates exceeding 200 °C/s. The aluminosilicate compositions were $NaAlSi_2O_6$, $Ca_{0.5}AlSi_2O_6$, and $Mg_{0.5}AlSi_2O_6$. Iron oxide was added in the form of Fe_2O_3, $NaFeO_2$, $CaFe_2O_4$, and $MgFe_2O_4$ with total iron oxide content in the range ~0.9 to ~5.6 mol% as Fe_2O_3. The Mössbauer spectra, which were deconvoluted by assuming Gaussian distributions of the hyperfine field, are consistent with one absorption doublet of Fe^{2+} and one of Fe^{3+}. From the area ratios of the Fe^{2+} and Fe^{3+} absorption doublets, with corrections for differences in recoil-fractions of Fe^{3+} and Fe^{2+}, the $Fe^{3+}/\Sigma Fe$ is positively correlated with increasing total iron content and with decreasing ionization potential of the alkali and alkaline earth cation. There is a distribution of hyperfine parameters from the Mössbauer spectra of these glasses. The maximum in the isomer shift distribution function of Fe^{3+}, $\delta_{Fe^{3+}}$, ranges from about 0.25 to 0.49 mm/s (at 298 K relative to Fe metal) with the quadrupole splitting maximum, $\Delta_{Fe^{3+}}$, ranging from ~1.2 to ~1.6 mm/s. Both $\delta_{Fe^{3+}}$ and $\delta_{Fe^{2+}}$ are negatively correlated with total iron oxide content and $Fe^{3+}/\Sigma Fe$. The dominant oxygen coordination number Fe^{3+} changes from 4 to 6 with decreasing $Fe^{3+}/\Sigma Fe$. The distortion of the Fe^{3+}–O polyhedra of the quenched melts (glasses) decreases as the $Fe^{3+}/\Sigma Fe$ increases. These polyhedra do, however, coexist with lesser proportions of polyhedra with different oxygen coordination numbers. The $\delta_{Fe^{2+}}$ and $\Delta_{Fe^{2+}}$ distribution maxima at 298 K range from ~0.95 to 1.15 mm/s and 1.9 to 2.0 mm/s, respectively, and decrease with increasing $Fe^{3+}/\Sigma Fe$. We suggest that these hyperfine parameter values for the most part are more consistent with Fe^{2+} in a range of coordination states from 4- to 6-fold. The lower $\delta_{Fe^{2+}}$-values for the most oxidized melts are consistent with a larger proportion of Fe^{2+} in 4-fold coordination compared with more reduced glasses and melts.

1. Introduction

Iron usually is the third-most abundant oxide in natural magmatic liquids (after SiO_2 and Al_2O_3). It occurs in two oxidation states, Fe^{3+} and Fe^{2+} with their redox ratio, $Fe^{3+}/\Sigma Fe$, depending on silicate composition, pressure, temperature, and oxygen fugacity.

Equilibrium between ferric and ferrous iron in silicate melt involves oxygen. Thus, the redox ratio of iron also affects the silicate melt structure (e.g., Mysen et al., 1984, 1985a; Dingwell and Virgo, 1987). Any silicate melt property that depends on melt structure, therefore, also depends on the redox ratio of iron whether or not this property is tied directly to iron content (see Mysen and Richet, 2005, Chapters 10 and 11, for recent review).

Whether in melts or minerals, the structural roles of Fe^{2+} and Fe^{3+} are often suggested to be different. In minerals, Fe^{2+} usually is in 6-fold coordination with oxygen. Only a few exceptions are known. The structural behavior of Fe^{2+} in silicate melts and glasses, on the other hand, is subject to debate with 4-, 5-, and 6-fold coordination with oxygen and a distribution of oxygen coordination numbers in proposed models (Calas and Petiau, 1983; Waychunas et al., 1988; Keppler, 1992; Wang et al., 1993; Burkhard, 2000; Rossano et al., 2000; Farges et al., 2004; Jackson et al., 2005).

* Fax: +1 202 478 8901.
E-mail address: mysen@gl.ciw.edu.

0016-7037/$ - see front matter © 2006 Elsevier Inc. All rights reserved.
doi:10.1016/j.gca.2006.01.026

Ferric iron in minerals normally also is in 6-fold coordination with oxygen, but a few examples of 4-fold coordinated Fe^{3+} exist (e.g., $KFeSi_3O_8$; see Henderson et al., 1984). In silicate melts and glasses, suggested coordination numbers of Fe^{3+} range from 4 to 6, as for Fe^{2+}. Available data suggest that 4-fold coordinated Fe^{3+} is more common, but a distribution of oxygen coordination is also possible (Mysen et al., 1980, 1985a; Virgo and Mysen, 1985; Alberto et al., 1996; Holland et al., 1999; Burkhard, 2000; Wilke et al., 2002; Farges et al., 2004).

The coordination state of Fe^{3+}, proportions of possible coexisting coordination states, and distortion of Fe^{3+}–O polyhedra may depend on the redox ratio as well as on other chemical factors (Virgo and Mysen, 1985; Dingwell and Virgo, 1987; Burkhard, 2000; Nagata and Hayashi, 2001; Jayasuriya et al., 2004). For example, variations of $Fe^{3+}/\Sigma Fe$ can cause the coordination state of Fe^{3+} to change (Virgo and Mysen, 1985; Dingwell and Virgo, 1987; Alberto, 1995). Thus, changes in parameters that affect $Fe^{3+}/\Sigma Fe$ can also result in coordination changes of ferric iron (Mysen and Virgo, 1989). This, in turn, affects the silicate melt structure. It has also been suggested that the Z/r^2 (ionization potential) of metal cations may affect the local iron–oxygen polyhedral geometry. This effect has been related to steric factors associated with charge-balance of tetrahedrally coordinated Fe^{3+} (Mysen et al., 1984, 1985a,b; Spiering and Seifert, 1985; Hannoyer et al., 1992; Nagata and Hayashi, 2001).

Less data exist for Fe^{2+}. It has been suggested that its coordination state may depend on silicate composition (Farges et al., 2004; Jackson et al., 2005). Whether these variations reflect changes in silicate composition and structure or variations in $Fe^{3+}/\Sigma Fe$ controlled by the melt and glass compositions is not known.

Substitution of Al^{3+} for Si^{4+} can also affect the structural environment around iron, in particular in oxidized alkali aluminosilicate melts (Mysen and Virgo, 1989). This effect could in part reflect competition for charge-balancing metal cations between tetrahedrally coordinated Fe^{3+} and Al^{3+} (typically alkalis and alkaline earths). In aluminosilicate melts, the relative stability of aluminate complexes and their activity–composition relations in aluminosilicate melts are related to the ionization potential of the charge-balancing cation (Roy and Navrotsky, 1984; Ryerson, 1985). Analogous relationships could exist for Fe^{3+}.

In order to shed further light on how ferric and ferrous iron dissolve in aluminosilicate melts and glasses, an experimental protocol with meta-aluminous melts was developed. Na-, Ca-, and Mg-meta-aluminosilicate melts were employed to address whether the form of charge-balance of tetrahedrally coordinated Al^{3+} affects the solubility behavior of Fe^{3+} and Fe^{2+}. In order to assess whether there may be competition between Fe^{3+} and Al^{3+} for potential charge-balancing cations with different electronic properties, in addition to adding iron simply as an oxide, it was also added in the nominal form of alkali- or alkaline earth-charge-balanced Fe^{3+} ($NaFeO_2$, $CaFe_2O_4$, and $MgFe_2O_4$).

2. Experimental methods

2.1. Starting compositions

To (i) address how Al^{3+} may affect the solubility mechanisms of ferrous and ferric iron, and (ii) to avoid complexity that may arise from a significant abundance of nonbridging oxygen, the Fe-free compositions were on the meta-aluminosilicate join with $Al/(Al + Si)$ near that of jadeite stoichiometry. The charge-balancing cations, Na^+, Ca^{2+}, and Mg^{2+}, were used to form $NaAlSi_2O_6$, $Ca_{0.5}AlSi_2O_6$, and $Mg_{0.5}AlSi_2O_6$ compositions. In the absence of iron these melts would nominally be considered nearly fully polymerized as charge-balanced Al^{3+} commonly is in tetrahedral coordination in substitution for Si^{4+} (e.g., Taylor and Brown, 1979; Matson et al., 1986; Neuville and Mysen, 1996). However, some recent data suggest that meta-aluminosilicate glasses may contain several percent nonbridging oxygen resulting from formation of Al-triclusters in the structure (Stebbins and Xue, 1997; Toplis et al., 2000; Neuville et al., 2004).

Iron oxide was added so that for each of the aluminosilicates, their nominal $Fe/(Fe + Al)$ ranged between 0.05 and 0.266 (Table 1). Increasing $Fe/(Fe + Al)$ is, therefore, also correlated with increasing total iron oxide content (Fig. 1). The $Al/(Al + Si)$ is known to affect the structural roles and redox relations of Fe^{3+} and Fe^{2+} (e.g., Mysen et al., 1985a; Mysen and Virgo, 1989). The $Al/(Al + Si)$ was, therefore, kept nearly constant [the average $Al/(Al + Si)$-value of all samples is 0.36 ± 0.03; see also Table 1].

2.2. Sample preparation

The starting materials were made from oxide (SiO_2, Al_2O_3, and MgO) and carbonate mixtures (Na_2CO_3 and $CaCO_3$). Iron oxide was added as Fe_2O_3 with some of the natural iron replaced with $^{57}Fe_2O_3$ to enhance the sensitivity of ^{57}Fe resonant Mössbauer absorption spectroscopy of the quenched melts (glasses). These mixtures (about 1 g total) were ground under alcohol for 60 min and kept at ~250 °C until used.

The starting materials were transformed to glass by melting at 1500 °C in air at ambient pressure and quenched to a glass in liquid H_2O. The samples were suspended on 0.1 mm diameter Pt wire loops (Presnall and Brenner, 1974) and brought to the desired temperature in $MoSi_2$-heated, vertical furnaces (Deltech Model 31C). The Pt wire was pre-saturated with iron before use. Approximately 20–30 mg sample was used for each experiment. All samples quenched to a clear glass without evidence of quench crystallization based on examination in a petrographic microscope at 500× magnification.

2.3. Mössbauer spectroscopy

The structural roles of Fe^{2+} and Fe^{3+} and the redox ratio of iron, $Fe^{3+}/\Sigma Fe$, of the quenched melts (glass) were

Table 1
Composition of glasses, wt%

	$NaAlSi_2O_6 + Fe_2O_3$				$NaAlSi_2O_6 + NaFeO_2$				
	OX1	OX4	OX5	OX6	OX13	OX14	OX15	OX16	OX50
SiO_2	57.25	55.23	53.01	50.02	56.84	54.01	50.22	46.24	41.27
Al_2O_3	24.89	24.21	25.22	25.31	25.04	24.95	24.96	25.34	24.94
Fe_2O_3	1.98	4.21	6.84	9.71	1.89	4.18	6.95	9.42	13.99
MgO	0	0	0	0	0	0	0	0	0
CaO	0	0	0	0	0	0	0	0	0
Na_2O	14.55	14.94	14.34	15.01	15.14	16.22	17.01	17.86	19.02
Total	98.67	98.59	99.41	100.05	98.91	99.36	99.14	98.86	99.22
	$NaAlSi_2O_6 + CaFe_2O_4$				$NaAlSi_2O_6 + MgFe_2O_4$				
	OX17	OX18	OX19	OX20	OX51	OX21	OX22	OX23	OX24
SiO_2	56.95	52.99	50.36	47.26	41.01	57.04	53.86	51.31	48.11
Al_2O_3	24.99	25.24	25.13	25.22	25.18	24.85	24.85	25.14	25.14
Fe_2O_3	1.91	4.12	6.84	9.46	13.89	1.94	4.12	6.76	9.65
MgO	0	0	0	0	0	0.41	0.79	1.41	2.14
CaO	0.54	1.23	1.86	2.68	3.54	0	0	0	0
Na_2O	15.23	15.54	15.24	15.31	14.86	14.84	15.24	15.04	15.05
Total	99.62	99.12	99.43	99.93	98.48	99.08	98.86	99.66	100.09
	$Ca_{0.5}AlSi_2O_6 + Fe_2O_3$				$Ca_{0.5}AlSi_2O_6 + NaFeO_2$				
	OX2	OX7	OX8	OX9	OX25	OX26	OX27	OX28	
SiO_2	59.36	55.76	53.47	50.12	57.32	54.38	51.26	46.86	
Al_2O_3	25.86	25.44	25.42	25.64	25.37	25.14	25.67	24.94	
Fe_2O_3	1.99	4.12	6.98	9.87	2.07	4.26	7.02	9.84	
MgO	0	0	0	0	0	0	0	0	
CaO	12.41	13.88	13.98	14.22	13.83	14.01	14	14.52	
Na_2O	0	0	0	0	0.56	1.14	1.89	2.68	
Total	99.62	99.2	99.85	99.85	99.15	98.93	99.84	98.84	
	$Ca_{0.5}AlSi_2O_6 + CaFe_2O_4$				$Ca_{0.5}AlSi_2O_6 + MgFe_2O_4$				
	OX29	OX30	OX31	OX32	OX33	OX34	OX35	OX36	
SiO_2	58.01	47.51	51.45	47.98	58.13	54.887	43.02	48.21	
Al_2O_3	25.64	22.33	25.47	25.84	25.61	24.96	37.99	25.43	
Fe_2O_3	1.91	3.64	6.89	9.81	1.89	4.26	5.454	9.87	
MgO	0	0	0	0	0.56	0.92	1.16	2.12	
CaO	14.31	25.61	15.99	16.28	14.22	14.23	11.55	14.22	
Na_2O	0	0	0	0	0	0	0	0	
Total	99.87	99.09	99.8	99.91	100.41	99.257	99.174	99.85	
	$Mg_{0.5}AlSi_2O_6 + Fe_2O_3$				$Mg_{0.5}AlSi_2O_6 + NaFeO_2$				
	OX3	OX10	OX11	OX12	OX37	OX38	OX39	OX40	
SiO_2	61.04	58.05	55.61	52.38	60.13	56.21	53.31	49.23	
Al_2O_3	26.29	26.47	26.41	26.54	26.83	26.47	26.73	26.47	
Fe_2O_3	1.99	4.53	7.23	10.21	1.95	4.38	6.86	10.12	
MgO	10.61	10.42	10.57	10.47	10.56	10.41	10.21	10.32	
CaO	0	0	0	0	0	0	0	0	
Na_2O	0	0	0	0	0.52	1.19	2.04	2.87	
Total	99.93	99.47	99.82	99.6	99.99	98.66	99.15	99.01	
	$Mg_{0.5}AlSi_2O_6 + Fe_2O_3$				$Mg_{0.5}AlSi_2O_6 + NaFeO_2$				
	OX41	OX42	OX43	OX44	OX45	OX47	OX48		
SiO_2	59.86	58.87	55.89	54.26	60.26	53.88	50.24		
Al_2O_3	26.91	25.84	24.78	23.74	26.41	26.14	26.13		
Fe_2O_3	2.14	4.02	6.54	8.87	1.85	6.82	10.22		
MgO	10.04	10.41	10.14	9.64	10.79	12.01	12.42		
CaO	0.57	1.16	1.85	2.51	0	0	0		
Na_2O	0	0	0	0	0	0	0		
Total	99.52	100.3	99.2	99.02	99.31	98.85	99.01		

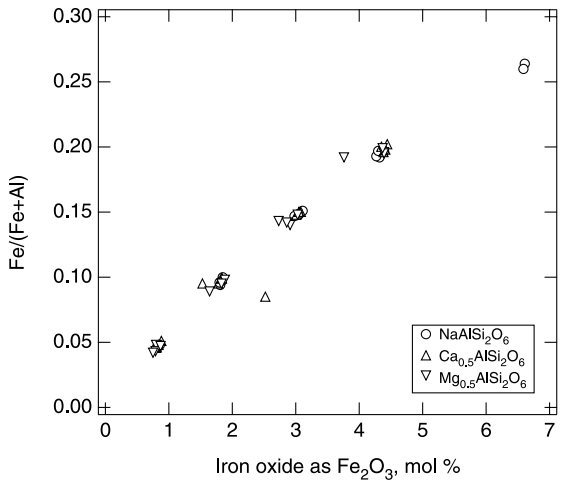

Fig. 1. Relationship between total iron oxide added (calculated as mol% Fe_2O_3) and Fe/(Fe + Al) of starting materials.

determined with ^{57}Fe resonant absorption Mössbauer spectroscopy. The samples were prepared by crushing a portion of the glass to a fine powder and mixed with transoptic powder. This mixture was converted to 12.7-mm diameter pellets at 350 bar and 120 °C. The resulting pellets, containing about 10–15 mg sample and about 100 mg transoptic powder, were about 1 mm thick.

The Mössbauer experiments were conducted with a ~40 mCi ^{57}Co flat source with the drives (Austin Science) operating in constant acceleration mode between −4 and 4 mm/s. Spectra were obtained at 298 and 77 K. The drives were calibrated with metallic Fe. The isomer shifts of Fe^{3+} and Fe^{2+}, $\delta_{Fe^{3+}}$ and $\delta_{Fe^{2+}}$, are reported relative to Fe metal.

The $Fe^{3+}/\Sigma Fe$ ratio can be obtained from the relative areas of the ferrous and ferric absorption doublets in the Mössbauer spectra. If we use only the 298 K Mössbauer data, the redox ratio thus derived relies on the assumption that the recoil-free fraction of Fe^{2+} and Fe^{3+} in the glasses is the same. A comparison of redox ratios obtained in this manner (spectra taken at 298 K) with redox ratios from wet chemical methods (Mysen et al., 1985c; Dingwell, 1991; Jayasuriya et al., 2004; Partzsch et al., 2004; see also Mysen and Richet, 2005, Fig. 10.3) indicates close correspondence between results with the two methods. There are, however, also data in the literature suggesting that this conclusion may not be entirely valid. From cryogenic Mössbauer measurements (77 K), Virgo and Mysen (1985) concluded that by using 298 K spectra only, Fe^{3+}/Fe^{2+} is over-estimated by about 5% (relative), a number similar to that reported by Mysen and Dubinsky (2004). In contrast, Jayasuriya et al. (2004) did not observe any effect of temperature on the redox ratio obtained with Mössbauer spectroscopy. These somewhat conflicting data, nevertheless, suggest that there may be a small effect on glass composition on the ratio of recoil-free fractions of Fe^{3+} and Fe^{2+}. For this reason, Mössbauer spectra, therefore, were recorded both at 298 K and 77 K.

2.4. Attainment of equilibrium

In these experiments, we used small samples (20–30 mg), which were inserted in the furnaces in the form of a fine powder (1–5 μm grain size). These pellets were kept in the CO–CO_2 gas flow at ~250 °C for about 10 min to ensure that air trapped between the grains was replaced with the gas mixture before the sample was inserted into the hot zone of the furnace. With this sample configuration, it has been found that 30 min is sufficient to reach equilibrium at temperatures comparable to those of the present experiments (Mysen et al., 1985a). The present experiments, all of which were at 1500 °C, were run for 60 min in order to ensure that equilibrium was reached.

2.5. Effect of quenching

The structure of a glass is that frozen in at its glass transition. The glass transition temperature depends on melt composition and quenching rate (e.g., Dingwell and Webb, 1990). Whether or not the redox ratio and structural state of ferric and ferrous iron reflect the state at the glass transition or that at the equilibration temperature of the melts has been the subject of several studies (e.g., Dyar et al., 1987; Wilke et al., 2002). Dyar et al. (1987) and Wilke et al. (2002) assessed the Mössbauer spectra of glasses as a function of quenching rate from high-temperature melt. With quenching rates in excess of 100–150 °C/s, the redox ratio of iron and the hyperfine parameters of ferric and ferrous iron were not affected by quenching. The quenching rate of the present samples is in excess of 200 °C/s. Thus, we conclude that the redox ratio of iron and the structural state of Fe^{2+} and Fe^{3+} in the quenched melts (glass) do not differ significantly from those in the melts. That conclusion is consistent with abundant data on systematic relations redox behavior of iron recorded for glass quenched from melt as a function of temperature and oxygen fugacity (see Chapters 10 and 11 in Mysen and Richet, 2005; for review of such data). Those relationships would not exist if they reflected conditions quenched in at the glass transition.

3. Experimental results

Iron-57 resonant absorption Mössbauer spectroscopy was employed to determine the redox ratio of ferric and ferrous iron (expressed as $Fe^{3+}/\Sigma Fe$ and Fe^{3+}/Fe^{2+} throughout this paper) and to provide information on the structural roles of Fe^{3+} and Fe^{2+} in the melts and glasses. All spectra recorded at 298 K exhibit absorption maxima near −0.5, 0.7, and 2 mm/s (Fig. 2). These features are typical for Mössbauer spectra of silicate glasses containing both Fe^{3+} and Fe^{2+} (e.g., Mysen and Virgo, 1978, 1989; Dyar et al., 1987; Alberto et al., 1993; Wang et al., 1993; Burkhard, 2000; Wilke et al., 2002: Jayasuriya et al., 2004; Farges et al., 2004). In these spectra, the low-velocity absorption maximum incorporates the low-velocity component of both the Fe^{3+} and the Fe^{2+} absorption doublet.

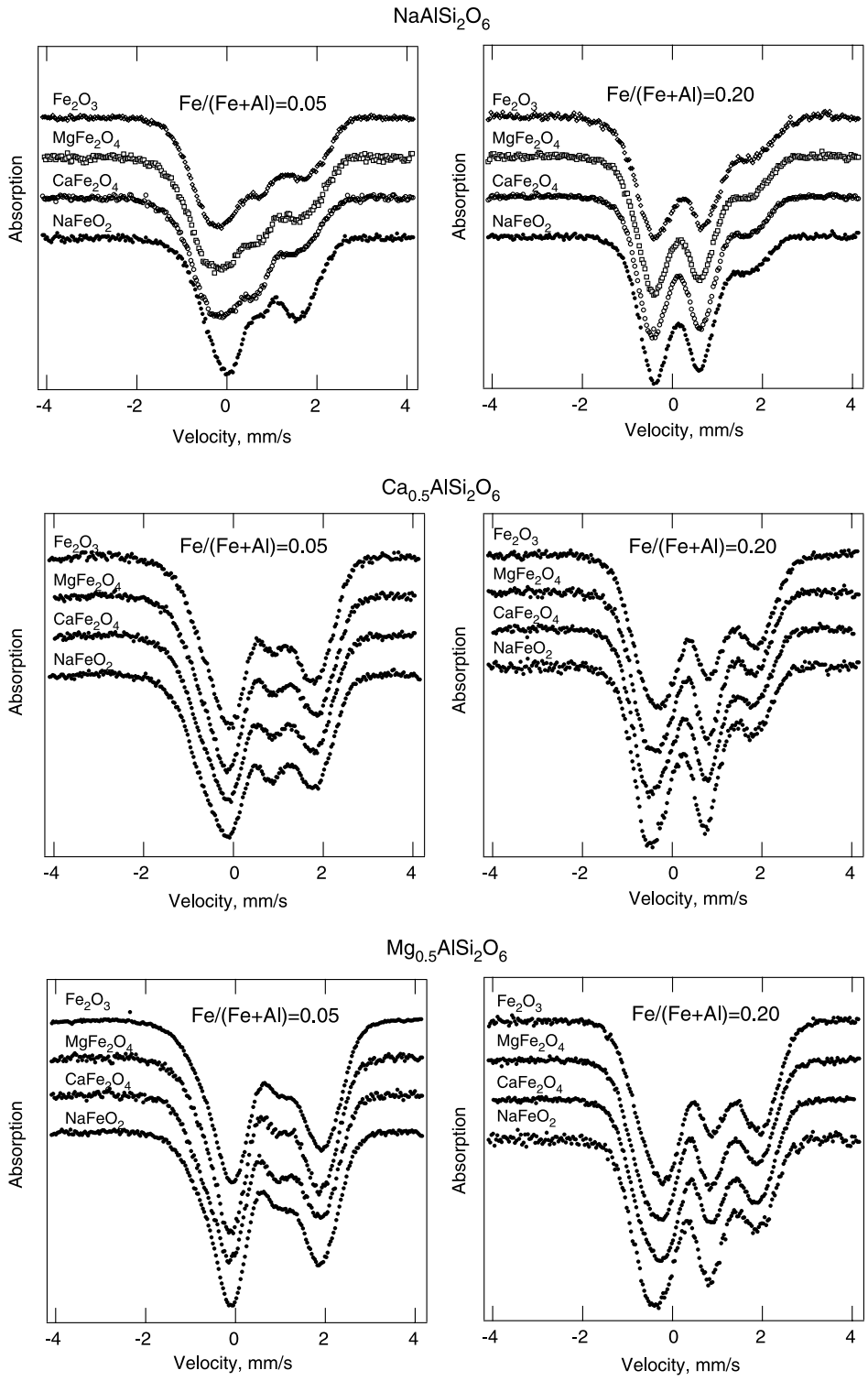

Fig. 2. ^{57}Fe resonant absorption Mössbauer spectra (recorded at 298 K) of compositions indicated in individual panels. The Fe/(Fe + Al) are approximate values. Exact values are reported in Table 1.

The maximum near 0.7 mm/s is due to the high-velocity component of the Fe^{3+} doublet, and that near 2 mm/s due to the high-velocity component of the Fe^{2+} doublet.

The relative intensities of the absorption maxima in Fig. 2 depend on the composition of the aluminosilicate, and the Fe/(Fe + Al) (and, therefore, total iron oxide content, see Fig. 1). The 0.7 mm/s maximum becomes stronger with increasing Fe/(Fe + Al), whereas the ~2 mm/s intensity decreases. A similar, though less pronounced, trend can be discerned as the aluminosilicate is changed from alkaline earth (Ca and Mg) to alkali (Na) aluminosilicate.

Table 2
Mössbauer data

Sample	Spectral temperature (K)	$Fe^{3+}/\Sigma Fe$	$\delta_{Fe^{3+}}$ (mm/s)	$\Delta_{Fe^{3+}}$ (mm/s)	$\delta_{Fe^{2+}}$ (mm/s)	$\Delta_{Fe^{2+}}$ (mm/s)	$w_{\delta_{Fe^{3+}}}$ (mm/s)	$w_{\Delta_{Fe^{3+}}}$ (mm/s)	$w_{\delta_{Fe^{2+}}}$ (mm/s)	$w_{\Delta_{Fe^{2+}}}$ (mm/s)
$NaAlSi_2O_6 + Fe_2O_3$										
OX1	298	0.48(2)[a]	0.301(5)	1.26(2)	0.994(8)	1.83(1)	0.31(1)	0.50(4)	0.411(7)	0.21(8)
OX1	*77*	*0.468(2)*	*0.428(2)*	*1.207(6)*	*0.11(4)*	*2.057(8)*	*0.30(2)*	*0.49(5)*	*0.437(5)*	*0.25(3)*
OX4	298	0.59(1)	0.281(1)	1.238(8)	0.982(5)	1.85(1)	0.21(3)	0.57(5)	0.36(1)	0.34(7)
OX4	*77*	*0.565(4)*	*0.394(3)*	*1.219(3)*	*1.071(4)*	*2.055(4)*	*0.25(3)*	*0.24(2)*	*0.35(2)*	*0.45(5)*
OX5	298	0.64(2)	0.266(4)	1.17(1)	0.972(9)	1.91(3)	0.24(1)	0.34(3)	0.34(4)	0.5(1)
OX5	*77*	*0.615(4)*	*0.359(7)*	*1.237(3)*	*1.093(3)*	*2.073(3)*	*0.300(4)*	*0.34(5)*	*0.30(2)*	*0.571(6)*
OX6	298	0.64(3)	0.253(9)	1.15(2)	0.95(7)	1.97(4)	0.21(5)	0.49(8)	0.38(3)	0.5(1)
OX6	*77*	*0.615(7)*	*0.356(1)*	*1.163(3)*	*1.00(3)*	*2.19(6)*	*0.22(1)*	*0.40(3)*	*0.48(4)*	*0.58(4)*
$NaAlSi_2O_6 + NaFeO_2$										
OX13	298	0.58(6)	0.33(2)	1.22(1)	1.080(6)	1.90(2)	0.29(3)	0.20(6)	0.23(2)	0.44(5)
OX13	*77*	*0.55(2)*	*0.430(5)*	*1.321(8)*	*1.180(6)*	*1.931(6)*	*0.35(1)*	*0.15(4)*	*0.25(4)*	*0.448(4)*
OX14	298	0.64(2)	0.290(9)	1.384(7)	1.082(4)	1.98(1)	0.348(7)	0.12(3)	0.25(2)	0.47(4)
OX15	298	0.713(3)	0.254(1)	1.092(2)	0.980(3)	1.701(3)	0.263(2)	0.18(2)	0.25 (1)	0.53(3)
OX16	298	0.71(1)	0.282(1)	1.071(4)	0.940(6)	1.900(9)	0.252(5)	0.11(4)	0.26(2)	0.45(5)
OX16	*77*	*0.705(6)*	*0.348(1)*	*1.101(2)*	*1.017(4)*	*2.100(7)*	*0.18(3)*	*0.25(6)*	*0.29(1)*	*0.38(5)*
OX50	298	0.809(5)	0.232(1)	1.063(2)	0.980(6)	1.64(2)	0.213(3)	0.16(1)	0.29(1)	0.22(8)
$NaAlSi_2O_6 + CaFe_2O_4$										
OX17	298	0.56(3)	0.280(4)	1.27(2)	0.98(2)	1.84(2)	0.25(3)	0.40(7)	0.45(2)	0.20(9)
OX18	298	0.607(9)	0.288(9)	1.156(4)	1.02(3)	2.00(3)	0.242(6)	0.26(1)	0.324(9)	0.11(3)
OX19	298	0.69(1)	0.251(1)	1.110(5)	0.98(1)	1.77(2)	0.25(2)	0.1(2)	0.38(2)	0.2(1)
OX19	*77*	*0.653(7)*	*0.336(1)*	*1.137(3)*	*1.080(6)*	*1.91(1)*	*0.19(6)*	*0.3(1)*	*0.43(1)*	*0.23(6)*
OX20	298	0.713(7)	0.266(9)	1.134(3)	0.985(9)	1.79(2)	0.22(1)	0.25(5)	0.37(1)	0.20(8)
OX51	298	0.79(2)	0.245(2)	1.135(4)	0.98(2)	1.64(2)	0.20(4)	0.3(1)	0.35(2)	0.2(1)
$NaAlSi_2O_6 + MgFe_2O_4$										
OX21	298	0.52(3)	0.276(2)	1.269(6)	0.995(5)	1.729(7)	0.34(2)	0.2(1)	0.25(5)	0.45(9)
OX22	298	0.62(2)	0.277(5)	1.214(7)	0.97(1)	1.80(1)	0.30(1)	0.12(1)	0.28(1)	0.24(5)
OX23	298	0.69(1)	0.253(3)	1.180(6)	0.998(8)	1.91(1)	0.285(6)	0.16(4)	0.28(6)	0.3(2)
OX24	298	0.68(1)	0.264(6)	1.098(4)	0.910(9)	1.85(1)	0.265(6)	0.11(5)	0.30(2)	0.2(1)
$Ca_{0.5}AlSi_2O_6 + Fe_2O_3$										
OX2	298	0.39(3)	0.34(4)	1.46(9)	1.074(3)	1.881(4)	0.22(1)	0.72(4)	0.17(5)	0.51(7)
OX2	*77*	*0.41(3)*	*0.530(3)*	*1.58(5)*	*1.224(3)*	*2.138(7)*	*0.26(7)*	*0.9(1)*	*0.27(3)*	*0.56(6)*
OX7	298	0.43(2)	0.30(4)	1.49(9)	1.074(3)	1.952(5)	0.21(2)	0.66(4)	0.17(8)	0.5(1)
OX7	*77*	*0.42(1)*	*0.457(7)*	*1.518(9)*	*1.194(2)*	*2.186(6)*	*0.25(4)*	*0.70(6)*	*0.16(1)*	*0.34(3)*
OX8	298	0.48(2)	0.29(2)	1.46(4)	1.063(3)	1.923(5)	0.20(5)	0.54(5)	0.19(6)	0.51(9)
OX8	*77*	*0.462(5)*	*0.429(3)*	*1.461(5)*	*1.19(1)*	*2.160(3)*	*0.29(2)*	*0.55(3)*	*0.23(2)*	*0.37(1)*
OX9	298	0.49(2)	0.28(2)	1.46(2)	1.061(3)	1.949(4)	0.21(5)	0.52(5)	0.20(5)	0.51(7)
OX9	*77*	*0.48(1)*	*0.424(7)*	*1.45(1)*	*1.182(4)*	*2.19(1)*	*0.31(4)*	*0.54(7)*	*0.26(1)*	*0.41(4)*
$Ca_{0.5}AlSi_2O_6 + NaFeO_2$										
OX25	298	0.48(2)	0.276(7)	1.549(5)	1.069(3)	1.908(4)	0.365(7)	0.64(4)	0.17(5)	0.49(8)
OX26	298	0.54(1)	0.258(2)	1.454(2)	1.045(2)	1.923(3)	0.292(2)	0.60(1)	0.19(1)	0.44(2)
OX27	298	0.62(1)	0.292(6)	1.364(8)	1.04(1)	1.960(5)	0.314(5)	0.61(2)	0.22(4)	0.55(8)
OX28	298	0.66(2)	0.29(1)	1.27(1)	1.02(4)	2.03(2)	0.27(1)	0.57(6)	0.24(8)	0.6(2)
$Ca_{0.5}AlSi_2O_6 + CaFe_2O_4$										
OX29	298	0.48(2)	0.292(7)	1.555(3)	1.074(3)	1.912(5)	0.382(5)	0.61(2)	0.14(6)	0.48(2)
OX30	298	0.514(7)	0.296(2)	1.432(2)	1.041(1)	2.080(3)	0.37(1)	0.74(2)	0.259(9)	0.47(2)
OX31	298	0.571(7)	0.267(2)	1.436(2)	1.051(2)	1.899(2)	0.281(4)	0.63(3)	0.17(3)	0.49(4)
OX32	298	0.61(1)	0.270(3)	1.400(3)	1.040(3)	1.891(5)	0.257(9)	0.62(7)	0.21(5)	0.46(5)
$Ca_{0.5}AlSi_2O_6 + MgFe_2O_4$										
OX33	298	0.46(1)	0.303(6)	1.566(4)	1.088(2)	1.964(4)	0.395(6)	0.63(2)	0.16(2)	0.51(3)
OX34	298	0.51(1)	0.295(4)	1.488(3)	1.055(3)	1.927(3)	0.308(6)	0.60(5)	0.18(3)	0.48(5)
OX35	298	0.52(1)	0.269(3)	1.463(3)	1.063(2)	1.972(3)	0.305(6)	0.66(4)	0.15(2)	0.50(2)
OX36	298	0.60(1)	0.283(4)	1.424(4)	1.056(3)	1.904(5)	0.261(7)	0.62(5)	0.15(3)	0.46(1)
$Mg_{0.5}AlSi_2O_6 + Fe_2O_3$										
OX3	298	0.30(1)	0.41(3)	1.58(6)	1.136(1)	1.979(1)	0.145(9)	0.68(2)	0.22(1)	0.47(2)
OX3	*77*	*0.28(3)*	*0.539(8)*	*1.547(5)*	*1.197(2)*	*2.163(4)*	*0.24(5)*	*0.77(6)*	*0.26(3)*	*0.50(6)*
OX10	298	0.36(1)	0.37(4)	1.57(6)	1.101(1)	1.968(1)	0.14(1)	0.58(4)	0.22(3)	0.45(5)
OX10	*77*	*0.346(9)*	*0.48(5)*	*1.63(9)*	*1.253(1)*	*2.162(2)*	*0.152(8)*	*0.65(4)*	*0.26(3)*	*0.52(6)*
OX11	298	0.410(8)	0.36(2)	1.55(3)	1.108(1)	2.011(2)	0.16(2)	0.56(4)	0.22(1)	0.47(2)

Table 2 (*continued*)

Sample	Spectral temperature (K)	$Fe^{3+}/\Sigma Fe$	$\delta_{Fe^{3+}}$ (mm/s)	$\Delta_{Fe^{3+}}$ (mm/s)	$\delta_{Fe^{2+}}$ (mm/s)	$\Delta_{Fe^{2+}}$ (mm/s)	$w_{\delta_{Fe^{3+}}}$ (mm/s)	$w_{\Delta_{Fe^{3+}}}$ (mm/s)	$w_{\delta_{Fe^{2+}}}$ (mm/s)	$w_{\Delta_{Fe^{2+}}}$ (mm/s)
OX11	*77*	*0.376(7)*	*0.4(2)*	*1.5(4)*	*1.234(9)*	*2.21(2)*	*0.17(3)*	*0.60(4)*	*0.25(1)*	*0.49(2)*
OX12	298	0.42(1)	0.36(3)	1.48(7)	1.094(2)	1.998(3)	0.12(1)	0.56(3)	0.17(6)	0.54(7)
OX12	*77*	*0.40(1)*	*0.44(2)*	*1.56(4)*	*1.260(2)*	*2.205(5)*	*0.17(6)*	*0.56(8)*	*0.26(3)*	*0.49(6)*
$Mg_{0.5}AlSi_2O_6 + NaFeO_2$										
OX37	298	0.32(2)	0.38(2)	1.57(4)	1.098(2)	1.969(2)	0.15(1)	0.68(2)	0.15(2)	0.50(3)
OX38	298	0.43(2)	0.31(2)	1.55(3)	1.08(3)	1.963(4)	0.14(4)	0.54(5)	0.11(5)	0.57(4)
OX39	298	0.47(2)	0.309(3)	1.506(4)	1.084(2)	1.995(4)	0.14(2)	0.53(2)	0.12(1)	0.56(1)
OX40	298	0.54(3)	0.30(1)	1.45(2)	1.055(5)	1.98(1)	0.13(7)	0.48(8)	0.13(3)	0.53(2)
$Mg_{0.5}AlSi_2O_6 + CaFe_2O_4$										
OX41	298	0.36(3)	0.32(2)	1.61(6)	1.095(3)	1.972(4)	0.14(2)	0.63(3)	0.13(4)	0.53(4)
OX42	298	0.40(3)	0.32(1)	1.60(2)	1.101(3)	1.971(5)	0.15(4)	0.58(5)	0.16(2)	0.48(1)
OX43	298	0.46(2)	0.285(4)	1.552(4)	1.082(2)	1.983(3)	0.187(6)	0.56(7)	0.16(2)	0.49(3)
OX44	298	0.49(1)	0.284(2)	1.536(2)	1.080(1)	1.979(2)	0.178(2)	0.52(2)	0.17(2)	0.48(3)
$Mg_{0.5}AlSi_2O_6 + MgFe_2O_4$										
OX45	298	0.32(4)	0.38(2)	1.56(7)	1.092(3)	1.983(4)	0.12(2)	0.69(3)	0.15(2)	0.49(3)
OX47	298	0.47(2)	0.299(5)	1.532(5)	1.082(3)	1.994(5)	0.12(2)	0.50(4)	0.09(4)	0.53(1)
OX48	298	0.484(8)	0.31(2)	1.51(4)	1.069(2)	1.988(2)	0.13(2)	0.52(4)	0.06(1)	0.597(5)

Symbols: $Fe^{3+}/\Sigma Fe$, Ratio of Fe^{3+} over total iron ($Fe^{3+} + Fe^{2+}$); $\delta_{Fe^{3+}}$, isomer shift of Fe^{3+} corresponding to maximum of probability function; $\Delta_{Fe^{3+}}$, quadrupole splitting of Fe^{3+} corresponding to maximum of probability function; $\delta_{Fe^{2+}}$, isomer shift of Fe^{2+} corresponding to maximum of probability function; $\Delta_{Fe^{2+}}$, quadrupole splitting of Fe^{2+} corresponding to maximum of probability function; $w_{\delta_{Fe^{3+}}}$, full width at half height of probability function of isomer shift of Fe^{3+}; $w_{\Delta_{Fe^{3+}}}$, full width at half height of probability function of quadrupole splitting of Fe^{3+}; $w_{\delta_{Fe^{2+}}}$, full width at half height of probability function of isomer shift of Fe^{2+}; $w_{\Delta_{Fe^{2+}}}$, full width at half height of probability function of quadrupole splitting of Fe^{2+}.
Numbers in italics are from spectra recorded at 77 K.
[a] Number in parentheses denotes uncertainty from spectra deconvolution.

3.1. Spectral deconvolution

The Mössbauer spectra were deconvoluted to obtain the redox ratio of iron, the hyperfine parameters (quadrupole splitting, δ, and isomer shift, Δ), and their distribution. The deconvolution procedure employed the algorithm of Alberto et al. (1996), which in principle is similar to the approach advocated by Lagarec and Rancourt (1997) and Rossano et al. (1999). Similar deconvolution procedures were also used in the recent studies by Wilke et al. (2002) and Jayasuriya et al. (2004).

In this method, the site distribution function, $S_i(v)$, is related to the probability distribution function, $P(\delta_i, \Delta_i, \sigma_{\delta_i}, \sigma_{\Delta_i}, \theta_i)$, of the absorption doublet, $D(v, \delta_i, \Delta_i, \omega, I_i)$, as:

$$S_i(v) = \int\int P(\delta_i, \Delta_i, \sigma_{\delta_i}, \sigma_{\Delta_i}, \theta_i) \cdot D(v, \delta_i, \Delta_i, \omega, I_i)\, \mathrm{d}\delta_i\, \mathrm{d}\Delta_i. \quad (1)$$

Here, v is the velocity, δ_i and Δ_i are the isomer shift and quadrupole splitting, with respective standard deviations, σ_{δ_i} and σ_{Δ_i}. The intensity is I_i. The fitting is conducted with the width of the elementary absorption peaks, ω, kept constant and equal to that of elemental Fe. The θ_i is a correlation parameter between isomer shift and quadrupole splitting.

Briefly, the probability function is:

$$P(\delta, \Delta, \sigma_\delta, \delta_\Delta, \theta) = \frac{1}{2\pi\sigma_\delta\delta_\Delta}\left\{-\frac{1}{2}\left[\left(\frac{\delta'}{w_\delta}\right)^2 + \left(\frac{\Delta'}{w_\Delta}\right)^2\right]\right\}, \quad (2)$$

where δ' and Δ' are related to the average isomer shift, $\overline{\delta}$, isomer shift, δ, average quadrupole splitting, $\overline{\Delta}$, quadrupole splitting, Δ, and the correlation parameter, θ, as:

$$\delta' = (\delta - \overline{\delta})\cos\theta + (\Delta - \overline{\Delta})\sin\theta \quad (3)$$

and

$$\Delta' = (\delta - \overline{\delta})\sin\theta + (\Delta - \overline{\Delta})\cos\theta. \quad (4)$$

The relationship between δ (isomer shift) and Δ (quadrupole splitting) can be expressed as an ellipse centered at the average values of δ and Δ, and the widths are w_δ and w_Δ, respectively.

The absorption doublet, $D(v, \delta, \Delta, \omega, I)$, then is:

$$D(v, \delta, \Delta, \omega, I) = I\left[\frac{1}{1 + \frac{(v-\delta+\Delta/2)}{\omega^2/4}}\right] + \left[\frac{1}{1 + \frac{(v-\delta-\Delta/2)}{\omega^2/4}}\right]. \quad (5)$$

The number of site distributions was determined by evaluating the χ^2 from the resulting fit. For all the samples described here, the spectra were deconvoluted satisfactorily with one distribution for Fe^{3+} and one for Fe^{2+}. The parameters from these fits (redox ratio of iron, hyperfine parameters, and hyperfine parameter distribution) are given in Table 2. The hyperfine parameter values, δ and Δ, are those corresponding to the maximum in the probability function in Eq. (2). The full width at half height (FWHH) of the probability functions will be referred to as w_δ and w_Δ.

Examples of the total probability function, $P(\delta_i, \Delta_i, \sigma_{\delta_i}, \sigma_{\Delta_i}, \theta_i)$ (see Eqs. (1) and (2)), from such fits are shown in Fig. 3 with the deconvolution of the absorption

envelope shown in Fig. 4. There is a fairly wide distribution of quadrupole splitting and isomer shift for both Fe^{3+} and Fe^{2+} (Fig. 3). The FWHH of the probability functions of both isomer shift and quadrupole splitting typically is 0.1–0.7 mm/s (Table 2). These values are similar to those of Wilke et al. (2002) from Mössbauer spectra of hydrous SiO_2–$NaAlSi_3O_8$–$CaAl_2Si_2O_8$–H_2O–Fe–O glass, but differ from those of Alberto et al. (1996) from spectra of CaO–SiO_2–Fe–O glass. In the latter case, the isomer shift distribution of Fe^{3+} was narrower than that of the present study. It is not clear why this is so as there is no reason why there might not be an equally wide distribution of the hyperfine field of both Fe^{3+} and Fe^{2+}.

3.2. Temperature of Mössbauer data acquisition

The hyperfine parameters, their distribution, and redox ratio of iron (area ratio of absorption doublets—Fig. 4) from the fits to all the Mössbauer spectra recorded both at 298 and 77 K are given in Table 2. The values of the hyperfine param-

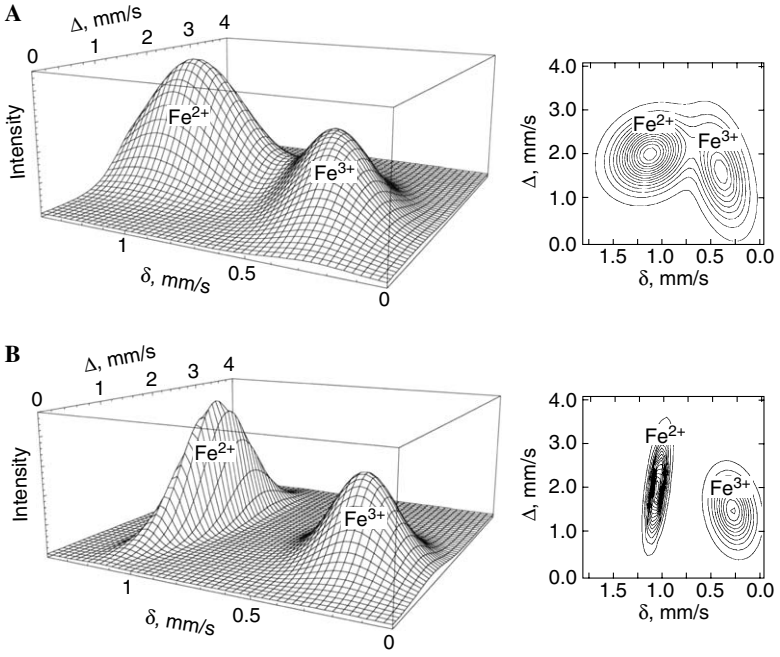

Fig. 3. Examples of the total probability functions of Mössbauer spectra of (A) sample OX3 [$Mg_{0.5}AlSi_2O_6 + Fe_2O_3$, with Fe/(Fe + Al) = 0.05], and (B) sample OX40 [$Mg_{0.5}AlSi_2O_6 + NaFeO_2$, with Fe/(Fe + Al) = 0.20]. Both spectra were recorded at 298 K. Left figures show the three-dimensional view, and right figures the intensity of the probability functions projected on the isomer shift (δ)/quadrupole splitting (Δ) surface.

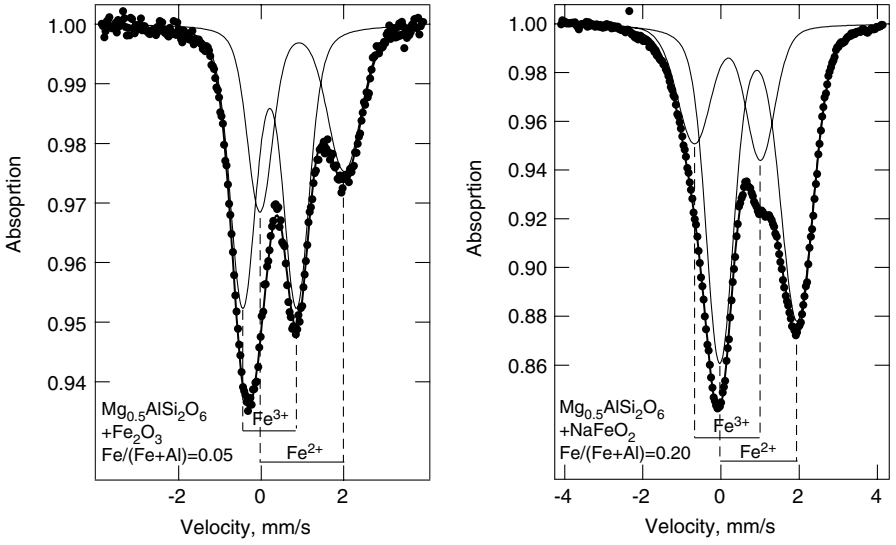

Fig. 4. The spectra used in Fig. 3 fitted to 2 two-dimensional Gaussian distributions. The absorption doublets assigned to Fe^{3+} and Fe^{2+} are marked in the figures.

eters and the area ratio of the absorption doublets depend on temperature during the Mössbauer data acquisition.

The isomer shift values change by between 5 and 10×10^{-4} mm/s K, a value in agreement with other data (e.g., Virgo and Mysen, 1985; Alberto, 1995). The area ratio of the absorption doublet, $A_{Fe^{3+}}/A_{Fe^{2+}}$, is consistently lower in the 77 K spectra than in the 298 K spectra. This difference reflects differences in recoil-free fraction of Fe^{3+} ($f_{Fe^{3+}}$) and Fe^{2+} ($f_{Fe^{2+}}$) of these glasses.

The area ratio, $A_{Fe^{3+}}/A_{Fe^{2+}}$, is related to the redox ratio, Fe^{3+}/Fe^{2+}, as:

$$Fe^{3+}/Fe^{2+} = (f_{Fe^{2+}}/f_{Fe^{3+}})(A_{Fe^{3+}}/A_{Fe^{2+}}). \quad (6)$$

The recoil-free fraction, f, at temperature, T, is (Alberto, 1995):

$$f = \exp[(\mathrm{d}(\ln A)/\mathrm{d}T)T]. \quad (7)$$

The ratio of recoil-free fractions, $f_{Fe^{2+}}/f_{Fe^{3+}}$, ranges from 0.83 to 0.96, with average values of 0.87 ± 0.02, 0.92 ± 0.02, and 0.89 ± 0.03, for $Mg_{0.5}AlSi_2O_6$, $Ca_{0.5}AlSi_2O_6$, and $NaAlSi_2O_6$ compositions, respectively (Table 3). Within uncertainty (standard error of the average), the $f_{Fe^{2+}}/f_{Fe^{3+}}$-ratio does not show any systematic relationship to the iron content [or Fe/(Fe + Al)] or on the form in which iron is added to the samples. In view of these observations, the actual Fe^{3+}/Fe^{2+}-ratios of the samples in the three aluminosilicate systems were corrected from the 298 K $Fe^{3+}/\Sigma Fe$-values in Table 2 with the average $f_{Fe^{3+}}/f_{Fe^{2+}}$-values in Table 3 via Eq. (6).

3.3. Redox relations and hyperfine parameters of ferric and ferrous iron

The $Fe^{3+}/\Sigma Fe$ of the glasses increases with total iron content regardless of silicate composition or the form in which iron was added (Fig. 5). An increase of $Fe^{3+}/\Sigma Fe$ with total iron content agrees with data for other compositions and iron contents (e.g., Larson and Chipman, 1953; Mysen et al., 1984; Lange and Carmichael, 1989; Kress and Carmichael, 1991).

The $Fe^{3+}/\Sigma Fe$ also depend on the composition of the silicate and to a much lesser extent the form in which the iron oxide was added. It decreases in the order $NaAlSi_2O_6 > Ca_{0.5}AlSi_2O_6 > Mg_{0.5}AlSi_2O_6$ (Fig. 5). In other words, the redox ratio of ion, $Fe^{3+}/\Sigma Fe$, decreases with Z/r^2 (ionization potential) of the cation that charge-balances Al^{3+} in tetrahedral coordination in the glasses and melts. This negative correlation is similar to that observed in other silicate melts whether the charge-balances cation tetrahedrally coordinated Al^{3+} or is a network-modifier in the melt (Paul and Douglas, 1965; Mysen et al., 1984, 1985a; Mysen and Virgo, 1989; Burkhard, 2000). The $Fe^{3+}/\Sigma Fe$-ratio depends slightly on whether iron oxide as added as Fe_2O_3 (no charge-balance) or in charge-balanced form (Fig. 5B). The type of charge-balancing cation does not, however, affect $Fe^{3+}/\Sigma Fe$.

The hyperfine parameters corresponding to the maximum in the probability function ($\delta_{Fe^{3+}}$, $\delta_{Fe^{2+}}$, $\Delta_{Fe^{3+}}$, and $\Delta_{Fe^{2+}}$) and hyperfine parameter distributions themselves ($w_{\delta_{Fe^{3+}}}$, $w_{\delta_{Fe^{2+}}}$, $w_{\Delta_{Fe^{3+}}}$, and $w_{\Delta_{Fe^{2+}}}$) depend on the composition of the glass (Table 2; Figs. 6 and 7). For ferric iron, the $\delta_{Fe^{3+}}$ in both the $NaAlSi_2O_6$ and $Ca_{0.5}AlSi_2O_6$ glasses for the most part is less than 0.3 mm/s at 298 K. For the Fe-bearing $Mg_{0.5}AlSi_2O_6$ melts, the $\delta_{Fe^{3+}}$ exceeds 0.4 mm/s for the samples with the lowest iron content. Regardless of the form in which iron oxide was added (Fe_2O_3, $NaFeO_2$, $CaFe_2O_4$, and $MgFe_2O_4$), the $\delta_{Fe^{3+}}$ remains nearly the same for each of the aluminosilicates (Fig. 6A; Table 4).

The $\delta_{Fe^{3+}}$ decreases slightly with increasing ferric iron content (Fig. 6). For a given total iron content $\delta_{Fe^{3+}}$ decreases in the order $Mg_{0.5}AlSi_2O_6 > Ca_{0.5}AlSi_2O_6 > NaAlSi_2O_6$. This relationship of $\delta_{Fe^{3+}}$ to cation properties is similar to those seen for other glass systems (Mysen et al., 1984, 1985a; Mysen and Virgo, 1989; Burkhard, 2000).

The full width at half height of the probability function of $\delta_{Fe^{3+}}$, $w_{\delta_{Fe^{3+}}}$, ranges from $\sim 0.15 \pm 0.05$ mm/s for glasses in the $Mg_{0.5}AlSi_2O_6$ system to 0.2–0.4 mm/s for glasses in the $Ca_{0.5}AlSi_2O_6$ and $NaAlSi_2O_6$ systems (Fig. 6A). The latter range diminishes somewhat with increasing Fe_2O_3 content. In none of the systems does the form in which iron oxide was added to the melt affect $w_{\delta_{Fe^{3+}}}$ significantly. Only the aluminosilicate composition has an effect on $w_{\delta_{Fe^{3+}}}$.

The quadrupole split values of Fe^{3+}, $\Delta_{Fe^{3+}}$ (Fig. 6B), show a more distinct separation between the three different aluminosilicate melts than does the isomer shift, $\delta_{Fe^{3+}}$ (Fig. 6A). The relationship is $\Delta_{Fe^{3+}(Mg0.5AlSi2O6)} > \Delta_{Fe^{3+}(Ca0.5AlSi2O6)} > \Delta_{Fe^{3+}(NaAlSi2O6)}$ with values near 1.6 mm/s for $Mg_{0.5}AlSi_2O_6$ melts and values near 1.5 and 1.2 mm/s for $Ca_{0.5}AlSi_2O_6$ and $NaAlSi_2O_6$ melts, respectively. The $\Delta_{Fe^{3+}}$-values decrease with increasing Fe_2O_3 content (Fig. 6B). There is no apparent effect on $\Delta_{Fe^{3+}}$ of the form

Table 3
Ratio of recoil-free fraction of ferrous and ferric iron, $f_{Fe^{2+}}/f_{Fe^{3+}}$, from Mössbauer measurements at 77 and 298 K (Table 2)

Sample	Composition	Fe/(Fe + Al)	$f_{Fe^{2+}}/f_{Fe^{3+}}$
OX1	$NaAlSi_2O_6 + Fe_2O_3$	0.05	0.93
OX4	$NaAlSi_2O_6 + Fe_2O_3$	0.1	0.86
OX5	$NaAlSi_2O_6 + Fe_2O_3$	0.15	0.87
OX6	$NaAlSi_2O_6 + Fe_2O_3$	0.2	0.88
OX13	$NaAlSi_2O_6 + NaFeO_2$	0.05	0.88
OX16	$NaAlSi_2O_6 + NaFeO_2$	0.2	0.96
OX19	$NaAlSi_2O_6 + NaFeO_2$	0.15	0.83
Average			0.89(2)[a]
OX2	$Ca_{0.5}AlSi_2O_6 + Fe_2O_3$	0.05	0.90
OX7	$Ca_{0.5}AlSi_2O_6 + Fe_2O_3$	0.1	0.93
OX8	$Ca_{0.5}AlSi_2O_6 + Fe_2O_3$	0.15	0.90
OX9	$Ca_{0.5}AlSi_2O_6 + Fe_2O_3$	0.2	0.95
Average			0.92(2)
OX3	$Mg_{0.5}AlSi_2O_6 + Fe_2O_3$	0.05	0.89
OX10	$Mg_{0.5}AlSi_2O_6 + Fe_2O_3$	0.1	0.90
OX11	$Mg_{0.5}AlSi_2O_6 + Fe_2O_3$	0.15	0.83
OX12	$Mg_{0.5}AlSi_2O_6 + Fe_2O_3$	0.2	0.85
Average			0.87(3)

[a] Number in parentheses denotes standard error of the average.

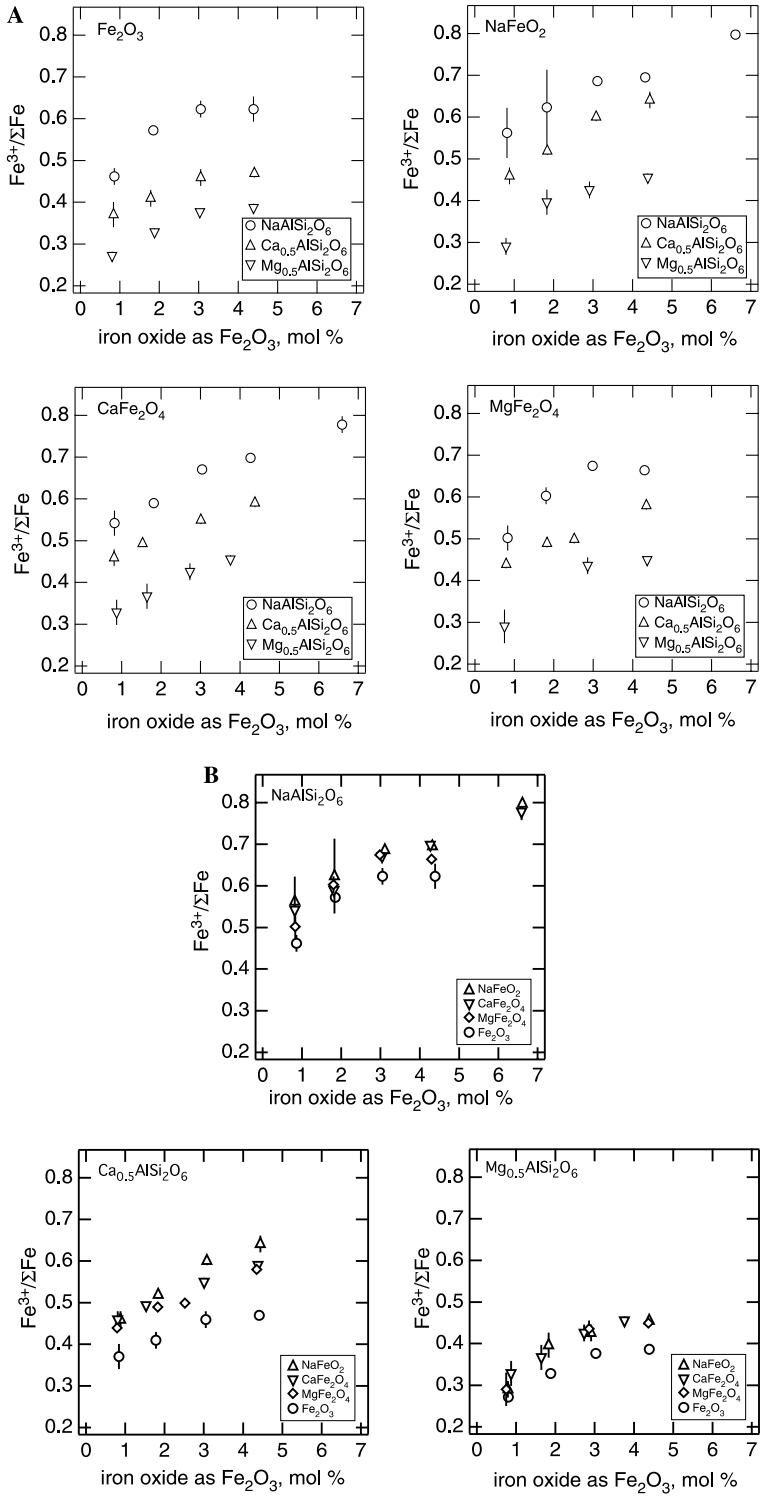

Fig. 5. Redox ratio of iron, $Fe^{3+}/\Sigma Fe$, (A) as a function total amount of iron oxide added (calculated as mol% Fe_2O_3) for the three aluminosilicate compositions with iron added as indicated in the panels, (B) as a function of the form in which iron oxide was added for the three aluminosilicate compositions. The redox ratio is that obtained after correction for the ratio of recoil-free fractions, $f_{Fe^{2+}}/f_{Fe^{3+}}$, as discussed in the text. These ratios are, therefore, slightly lower than those given in Table 2 (uncorrected Mössbauer data). Error bars from Mössbauer fitting errors. No error bar shown when error is smaller than symbol size.

in which iron oxide was added to the starting materials (Fe_2O_3, $NaFeO_2$, $CaFe_2O_4$, and $MgFe_2O_4$). The $w_{\Delta_{Fe^{3+}}}$ from the alkaline earth systems is tightly constrained near 0.6 mm/s, whereas for glasses in the $NaAlSi_2O_6$ system, the $w_{\Delta_{Fe^{3+}}}$ shows a wider range (Fig. 6B). The average value of $w_{\Delta_{Fe^{3+}}}$ from $NaAlSi_2O_6$ glass is, however, consistently

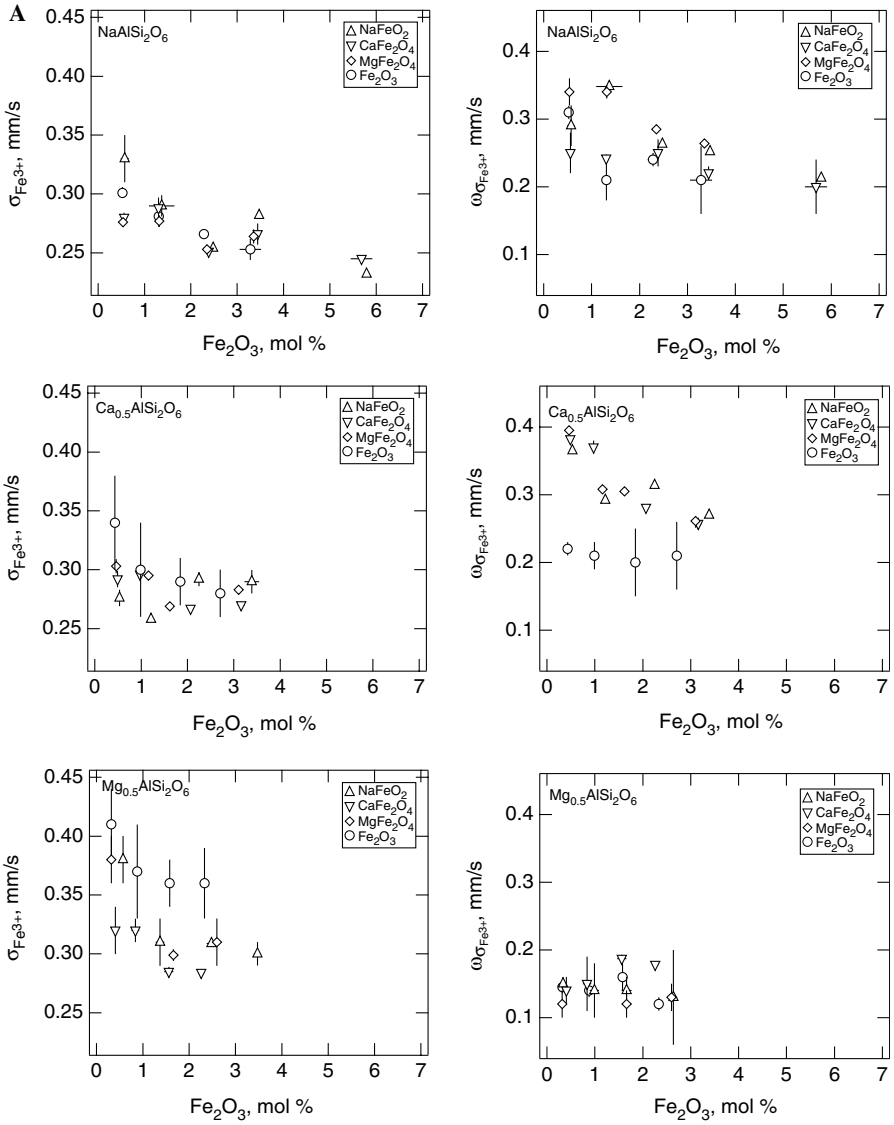

Fig. 6. (A) Isomer shift at maximum of probability function, $\delta_{Fe^{3+}}$, and full width at half height of isomer shift probability function quadrupole splitting, $w_{\delta_{Fe^{3+}}}$, of Fe^{3+} from 298 K spectra relative to Fe metal as a function of amount of measured ferric oxide content (as mol% Fe_2O_3) for compositions indicated in individual figures. (B) Quadrupole splitting at maximum of probability function, $\Delta_{Fe^{3+}}$, and full width at half height of quadrupole splitting probability function, $w_{\Delta_{Fe^{3+}}}$, of Fe^{3+} from 298 K spectra relative to Fe metal as a function of amount of measured ferric oxide content (as mol% Fe_2O_3) for compositions indicated in individual figures. The Fe_2O_3 content is that obtained after correction for the ratio of recoil-free fractions, $f_{Fe^{2+}}/f_{Fe^{3+}}$, as discussed in the text. Error bars from Mössbauer fitting errors. No error bar shown when error is smaller than symbol size.

lower than the values from $Ca_{0.5}AlSi_2O_6$ and $Mg_{0.5}AlSi_2O_6$ glasses (Table 4). As for $w_{\delta_{Fe^{3+}}}$ the $w_{\Delta_{Fe^{3+}}}$ decreases slightly with increasing Fe_2O_3 content at least in the alkaline earth systems (Figs. 6A and B).

The hyperfine parameters of Fe^{2+} are less sensitive to iron content than those of Fe^{3+} (Figs. 6 and 7). The values of both $\delta_{Fe^{2+}}$ and $\Delta_{Fe^{2+}}$ depend, however, on the aluminosilicate composition and increase in the order $Mg_{0.5}AlSi_2O_6 > Ca_{0.5}AlSi_2O_6 > NaAlSi_2O_6$ (Fig. 7), which is similar to the behavior of $\Delta_{Fe^{3+}}$ (Table 4). As for the isomer shift distribution of Fe^{3+}, the $w_{\delta_{Fe^{3+}}}$ from the alkaline earth glasses is more tightly constrained than for the alkali silicate glasses (Figs. 6A and 7A). Their $w_{\delta_{Fe^{2+}}}$-range and average values are also smaller than for $NaAlSi_2O_6$ glass (Fig. 7A; Table 4). The $w_{\Delta_{Fe^{2+}}}$-values also resemble the $w_{\Delta_{Fe^{3+}}}$ in that their range is narrower in the alkaline earth glasses than in $NaAlSi_2O_6$ (Fig. 7B). In contrast to $w_{\Delta_{Fe^{3+}}}$, the average $w_{\Delta_{Fe^{2+}}}$ of $NaAlSi_2O_6$ glasses is smaller than those of $Ca_{0.5}AlSi_2O_6$ and $Mg_{0.5}AlSi_2O_6$ (Table 4).

4. Discussion

The redox relations and hyperfine parameters of Fe^{3+} and Fe^{2+} are not dependent on the nature of Fe^{3+}-charge-balancing cations of the iron oxide dissolved in the glasses and melts. It seems, therefore, that for Fe^{3+} predominantly in tetrahedral coordination, some of the alkali or alkaline earth that charge-balance Al^{3+} in the aluminosilicate glasses

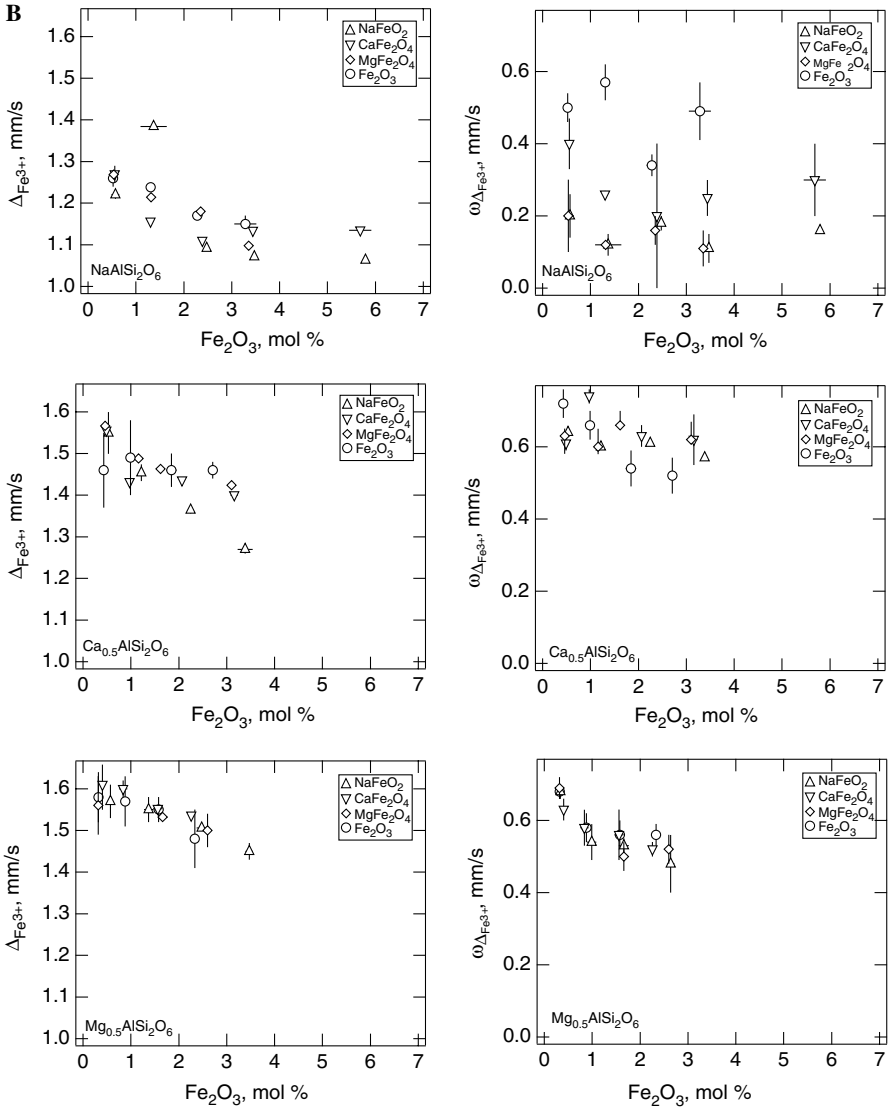

Fig. 6. (*continued*)

may be transferred to Fe^{3+} or Fe^{3+} in 4-fold coordination forms some form of a complex with Fe^{2+} as proposed, for example, by Virgo and Mysen (1985) and Kress and Carmichael (1991). There is, therefore, no evidence in the Mössbauer spectra that specific alkalis or alkaline earths may exhibit a preference for charge-balance of Al^{3+} and Fe^{3+} in tetrahedral coordination.

There is no single value of the hyperfine parameters of the Fe^{3+} and Fe^{2+} from the Mössbauer spectra of these glasses. Instead, there is a distribution of the δ- and Δ-values reflecting a distribution of the oxygen coordination numbers and the extent of distortion of the Fe^{3+}–O and Fe^{2+}–O polyhedra. A range in oxygen coordination numbers are consistent with other spectroscopic data suggesting the oxygen coordination numbers between 4 and 6 (Rossano et al., 2000; Wilke et al., 2002; Farges et al., 2004; Jackson et al., 2005). These ranges notwithstanding, there are distinct maxima in the probability functions of the Fe^{2+} and Fe^{3+} hyperfine field distributions (Fig. 3). The $\delta_{Fe^{3+}}$ and $\delta_{Fe^{2+}}$ maxima correspond to the most probable oxygen coordination number for Fe^{3+} and Fe^{2+}. The $\Delta_{Fe^{3+}}$ and $\Delta_{Fe^{2+}}$ maxima reflect the most probable extent of Fe^{3+}–O and Fe^{2+}–O polyhedral distortion.

4.1. Ferric iron

The $\delta_{Fe^{3+}}$-values may be compared with isomer shift values of Fe^{3+} in crystalline iron silicates to estimate the most probable coordination number of Fe^{3+} in the silicate glasses. For iron-bearing crystalline materials, there are systematic relations between the isomer shift and the oxygen coordination number (Burns, 1994). For Fe^{3+}, isomer shifts near 0.3 mm/s and below (at 298 K) are typical for Fe^{3+} in 4-fold coordination with oxygen, whereas values above about 0.4 mm/s are typical for Fe^{3+} in 6-fold coordination with oxygen. From these simple relationships, we

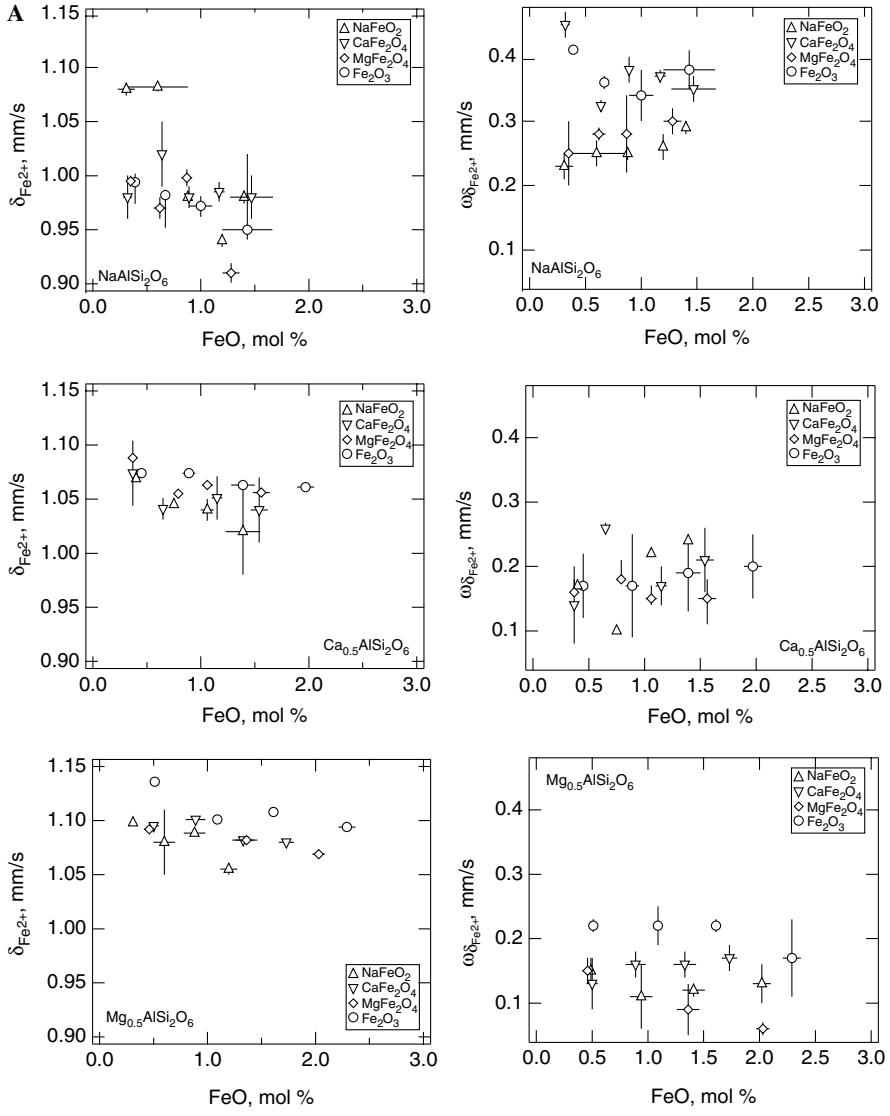

Fig. 7. (A) Isomer shift at maximum of probability function, $\delta_{Fe^{2+}}$, and full width at half height of isomer shift probability function quadrupole splitting, $w_{\delta_{Fe^{2+}}}$, of Fe^{2+} from 298 K spectra relative to Fe metal as a function of amount of measured ferric oxide content (as mol% FeO) for compositions indicated in individual figures. (B) Quadrupole splitting at maximum of probability function, $\Delta_{Fe^{2+}}$, and full width at half height of quadrupole splitting probability function, $w_{\Delta_{Fe^{2+}}}$, of Fe^{2+} from 298 K spectra relative to Fe metal as a function of amount of measured ferric oxide content (as mol% Fe_2O_3) for compositions indicated in individual figures. The FeO content is that obtained after correction for the ratio of recoil-free fractions, $f_{Fe^{2+}}/f_{Fe^{3+}}$, as discussed in the text. Error bars from Mössbauer fitting errors. No error bar shown when error is smaller than symbol size.

would conclude that Fe^{3+} in tetrahedral coordination is the most probable structure in all samples except some of the low-Fe $Mg_{0.5}AlSi_2O_6$ where the isomer shift exceeds 0.4 mm/s (Fig. 8). The latter values are consistent with higher oxygen coordination in those melts. Similar conclusions have been reported for other glass samples (Virgo and Mysen, 1985; Dingwell and Virgo, 1987; Jayasuriya et al., 2004). The correlation of $\delta_{Fe^{2+}}$ with the $Fe^{3+}/\Sigma Fe$ (Fig. 8A) agrees with earlier suggestions that the structural role of ferric iron in silicate glasses and melts depends on the ferric/ferrous ratio (O'Horo and Levy, 1978; Virgo and Mysen, 1985; Dingwell and Virgo, 1987; Kress and Carmichael, 1991). There remains, however, a distribution of $\delta_{Fe^{3+}}$-values regardless of $Fe^{3+}/\Sigma Fe$, which is consistent with a range of oxygen coordination numbers regardless of the oxidation state of the melt or glass. As the average $w_{\delta_{Fe^{3+}}}$ of $Mg_{0.5}AlSi_2O_6$ glass is smaller than those of $Ca_{0.5}AlSi_2O_6$ and $NaAlSi_2O_6$ (Table 4), the range of oxygen coordination numbers of Fe^{3+} in the $Mg_{0.5}AlSi_2O_6$ glasses is the smallest.

The most probable quadrupole split values are also sensitive to the redox ratio, $Fe^{3+}/\Sigma Fe$, and decrease with increasing $Fe^{3+}/\Sigma Fe$ (Fig. 8C). Thus, one may suggest that the extent of distortion of the Fe^{3+}–O polyhedra diminishes as the glasses become increasingly oxidized. There remains, however, a range in extent of polyhedral distortion as seen in the relationship between $w_{\Delta_{Fe^{3+}}}$ and $Fe^{3+}/\Sigma Fe$ (Fig. 8D). The range of distortion is smaller in

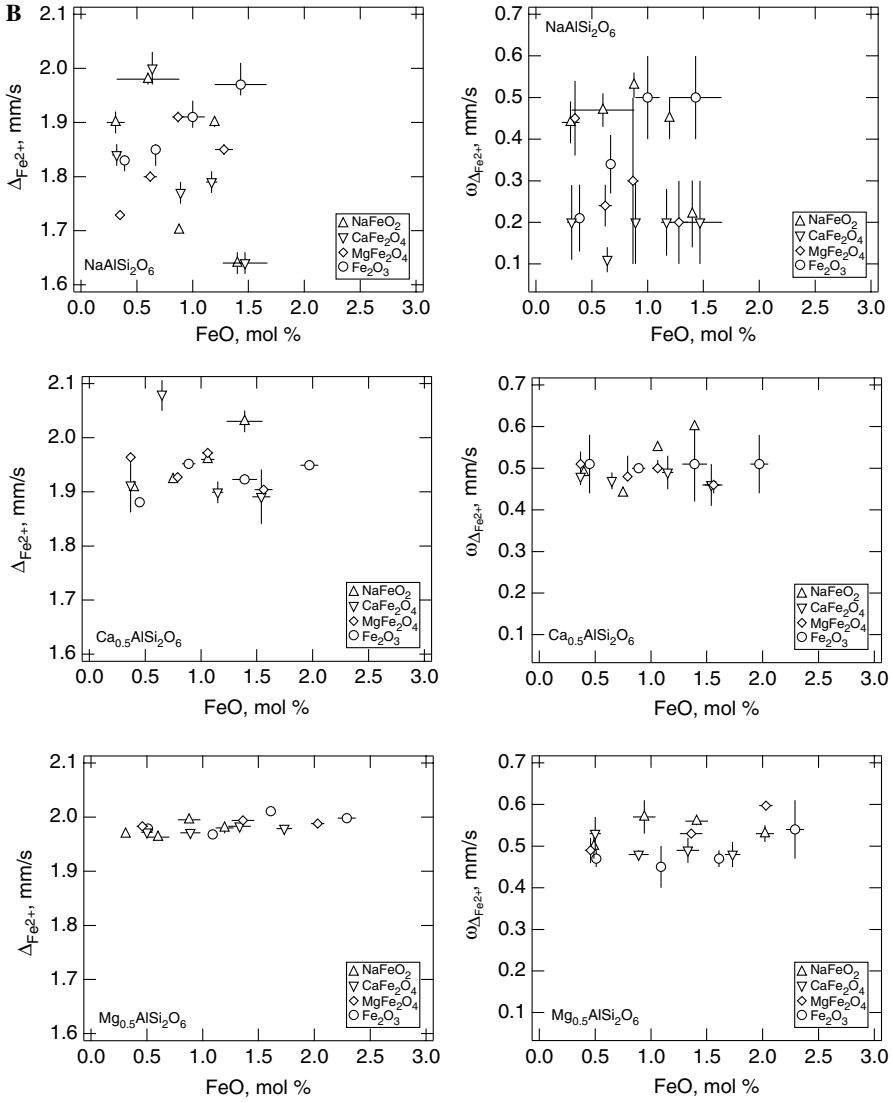

Fig. 7. (*continued*)

$NaAlSi_2O_6$ glasses than in $Ca_{0.5}AlSi_2O_6$ and $Mg_{0.5}AlSi_2O_6$ glasses (Fig. 6B; Table 4), which may reflect greater steric hindrance in the latter two glasses.

4.2. Ferrous iron

As for Fe^{3+}, a primary guide to the use of isomer shifts as an indicator of oxygen coordination numbers is the comparison with isomer shift values from crystalline Fe-bearing silicates. In the summary of such data by Burns (1994), $\delta_{Fe^{2+}}$ near 0.9 mm/s or less of crystalline Fe^{2+}-silicates is observed when Fe^{2+} is in 4-fold coordination. Values above 1 mm/s are found when Fe^{2+} is in 6-fold coordination with oxygen. Jackson et al. (2005) proposed that values intermediate between these $\delta_{Fe^{2+}}$-values may reflect ferrous iron in 5-fold coordination although they did not document this statement. Other suggestions for the coordination state of Fe^{2+} in silicate melts and glasses from other structural studies are, however, less than clear. For example, from an X-ray absorption study of another alkaline earth silicate glass, $2FeO \cdot 4MgO \cdot 4CaO \cdot SiO_2$, Calas and Petiau (1983) concluded that Fe^{2+} was in 4-fold coordination. Simulation of the structure of $CaFeSi_2O_6$ glass by Rossano et al. (2000) was interpreted to suggest that Fe^{2+} exists in 4- and 5-fold coordination. Waychunas et al. (1988) and Jackson et al. (1993) concluded similarly from X-ray absorption studies of Fe^{2+}-silicate glasses and melts. In contrast, optical absorption spectra of Fe^{2+}-silicate glasses commonly have been reported consistent with ferrous iron in 6-fold coordination (Bell and Mao, 1974; Nolet et al., 1979; Keppler, 1992), and, thus, is a network-modifier. Wang et al. (1993), from Raman data on $Na_2O \cdot SiO_2 \cdot FeO \cdot Fe_2O_3$ melts and glasses, also concluded that Fe^{2+} is a network-modifier.

The most probable $\delta_{Fe^{2+}}$-values from the Mössbauer spectra of the present glasses range from about 0.95 mm/s for the most Fe-rich $NaAlSi_2O_6$ glasses to as much as 1.15 mm/s for glasses in the $Mg_{0.5}AlSi_2O_6$ system (Table 2). There is an

Table 4
Average values of hyperfine parameters (δ and Δ) and their distributions (w_δ and w_Δ) (mm/s)

	$\delta_{Fe^{3+}}$	$w_{\delta_{Fe^{3+}}}$	$\Delta_{Fe^{3+}}$	$w_{\Delta_{Fe^{3+}}}$	$\delta_{Fe^{2+}}$	$w_{\delta_{Fe^{2+}}}$	$\Delta_{Fe^{2+}}$	$w_{\Delta_{Fe^{2+}}}$
$NaAlSi_2O_6 + Fe_2O_3$	0.28(2)[a]	0.24(5)	1.20(5)	0.5(1)	0.97(2)	0.37(3)	1.89(6)	0.4(1)
$Ca_{0.5}AlSi_2O_6 + Fe_2O_3$	0.30(2)	0.21(1)	1.47(2)	0.6(1)	1.068(7)	0.18(2)	1.93(3)	0.508(5)
$Mg_{0.5}AlSi_2O_6 + Fe_2O_3$	0.38(2)	0.14(2)	1.55(5)	0.59(6)	1.11(2)	0.21(3)	1.99(2)	0.48(4)
$NaAlSi_2O_6 + NaFeO_2$	0.28(3)	0.27(5)	1.2(1)	0.15(4)	1.01(6)	0.26(2)	1.8(1)	0.4(1)
$Ca_{0.5}AlSi_2O_6 + NaFeO_2$	0.28(2)	0.31(4)	1.4(1)	0.61(3)	1.04(2)	0.18(6)	1.96(5)	0.52(7)
$Mg_{0.5}AlSi_2O_6 + NaFeO_2$	0.33(4)	0.14(1)	1.52(5)	0.55(9)	1.08(2)	0.13(2)	1.98(1)	0.54(3)
$NaAlSi_2O_6 + CaFe_2O_4$	0.27(2)	0.23(2)	1.16(6)	0.28(8)	0.99(2)	0.37(5)	1.8(1)	0.18(4)
$Ca_{0.5}AlSi_2O_6 + CaFe_2O_4$	0.28(1)	0.32(6)	1.46(7)	0.65(6)	1.05(2)	0.19(5)	1.95(9)	0.48(1)
$Mg_{0.5}AlSi_2O_6 + CaFe_2O_4$	0.30(2)	0.16(2)	1.57(4)	0.57(5)	1.09(1)	0.16(2)	1.976(6)	0.50(2)
$NaAlSi_2O_6 + MgFe_2O_4$	0.27(1)	0.31(4)	1.19(7)	0.15(4)	0.97(4)	0.28(2)	1.82(8)	0.3(1)
$Ca_{0.5}AlSi_2O_6 + MgFe_2O_4$	0.29(1)	0.32(6)	1.49(6)	0.63(3)	1.07(2)	0.16(1)	1.94(3)	0.49(2)
$Mg_{0.5}AlSi_2O_6 + MgFe_2O_4$	0.33(4)	0.123(6)	1.53(3)	0.57(9)	1.08(1)	0.10(5)	1.988(6)	0.54(5)

[a] Number in parentheses denotes standard error of the average.

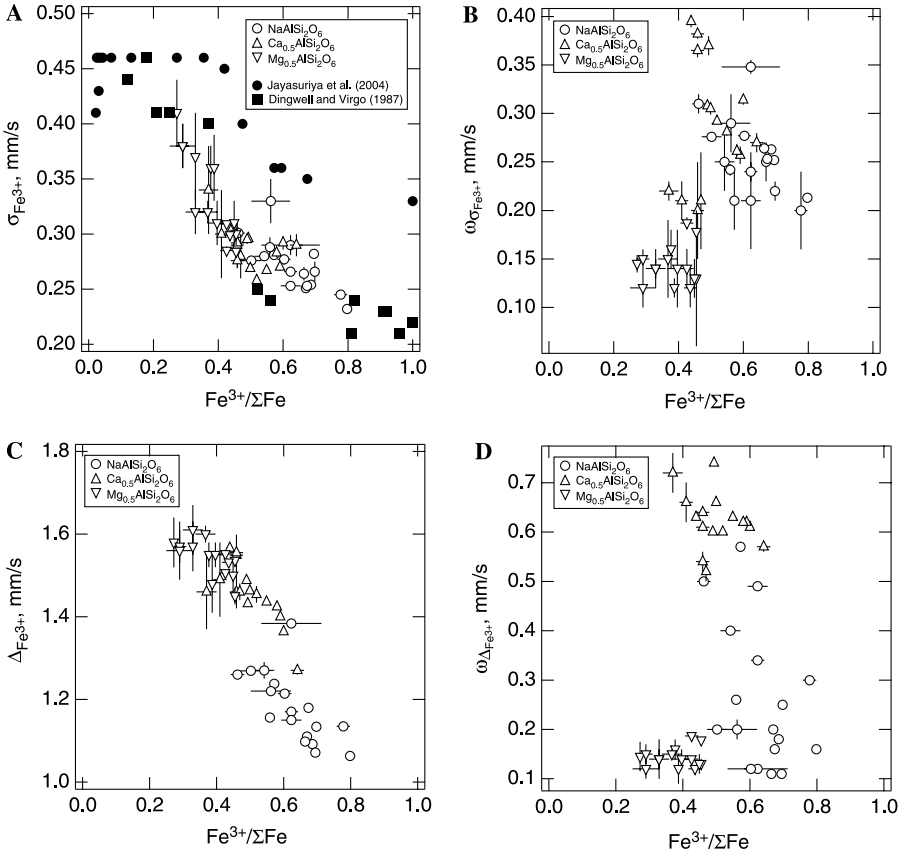

Fig. 8. Hyperfine parameters and their distributions of Fe^{3+} as a function of redox ratio, Fe^{3+}/Σ Fe. (A) Isomer shift at maximum of probability function, $\delta_{Fe^{3+}}$. (B) Isomer shift distribution, $w_{\delta_{Fe^{3+}}}$. (C) Quadrupole splitting at maximum of probability function, $\Delta_{Fe^{3+}}$. (D) Quadrupole splitting distribution, $w_{\Delta_{Fe^{3+}}}$.

increase of the most probable average $\delta_{Fe^{2+}}$-values from $NaAlSi_2O_6$, via $Ca_{0.5}AlSi_2O_6$, to $Mg_{0.5}AlSi_2O_6$ (Table 4). On this basis, one might conclude that Fe^{2+} exists in a range of coordination states, from something resembling 4 in the Fe-bearing $NaAlSi_2O_6$ system to 5- or 6-fold coordination in alkaline earth aluminosilicates ($Ca_{0.5}AlSi_2O_6$ and $Mg_{0.5}AlSi_2O_6$). Whether these relations are governed by the electronic properties of Na^+, Ca^{2+}, and Mg^{2+} in the aluminosilicate glasses or by Fe^{3+}/ΣFe, which depends on the same parameters (Fig. 5), is not clear. We note, however, that there is considerable overlap in the $\delta_{Fe^{2+}}$ vs. Fe^{3+}/ΣFe relations among the three aluminosilicate glasses (Fig. 9A). This overlap may suggest that the $\delta_{Fe^{2+}}$ is controlled by Fe^{3+}/ΣFe, which, in

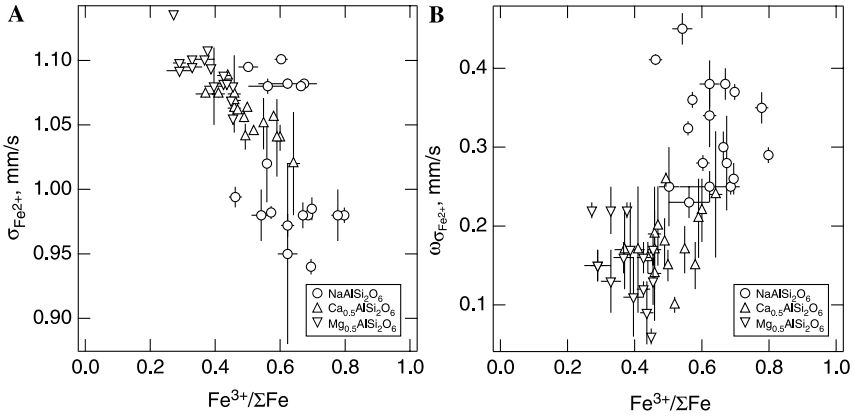

Fig. 9. Isomer shift and isomer shift distribution of Fe^{2+} as a function of redox ratio, $Fe^{3+}/\Sigma Fe$. (A) Isomer shift at maximum of probability function, $\delta_{Fe^{2+}}$. (B) Isomer shift distribution, $w_{\delta_{Fe^{2+}}}$.

turn is governed by the aluminosilicate composition. In other words, the oxygen coordination number around Fe^{2+} appears related to the redox ratio of iron and not the aluminosilicate composition. Whether the distribution of the coordination numbers, expressed as $w_{\delta_{Fe^{2+}}}$, also depends on $Fe^{3+}/\Sigma Fe$ is less clear (Fig. 9B).

The systematics of the most probable oxygen coordination numbers of Fe^{2+} notwithstanding, the present Mössbauer data are consistent with suggestions that there is a range of oxygen coordination numbers around the most probable value. This conclusion in principle is in accord with other recent suggestions of Rossano et al. (1999), Farges et al. (2004), and Jackson et al., 2005). The systematic relationships between the most probable coordination number, expressed as $\delta_{Fe^{2+}}$, and $Fe^{3+}/\Sigma Fe$ lead to the conclusion that the increasing $Fe^{3+}/\Sigma Fe$ is associated with smaller coordination numbers of Fe^{2+}.

5. Concluding remarks

1. The redox ratio of iron in silicate glasses (and probably melts), $Fe^{3+}/\Sigma Fe$, is a positive function of the total iron content. Its value in aluminosilicate glasses does, however, depend on the electronic properties of the cation serving to charge-balance Al^{3+} in tetrahedral coordination. This relationship is qualitatively similar to that of depolymerized silicate glasses, where electronic properties of network-modifying cations have similar effect on $Fe^{3+}/\Sigma Fe$.
2. The probability functions of the hyperfine parameters are consistent with a range of coordination states and extent of distortion of iron–oxygen polyhedra in glasses. This range decreases somewhat with increasing iron content of the glasses. However, the most probable coordination states (from isomer shifts) of both Fe^{3+} and Fe^{2+} are systematic functions of $Fe^{3+}/\Sigma Fe$. Increasing $Fe^{3+}/\Sigma Fe$ causes a decrease in the coordination number of both Fe^{2+} and Fe^{3+}. The extent of polyhedral distortion (from quadrupole splitting) appears less sensitive to the redox state of iron. However, both Fe^{3+}–O and Fe^{2+}–O polyhedra become increasingly distorted as the ionization potential of alkali and alkaline earths in the system increases.

Acknowledgment

Support from NSF Grant EAR0405383 is appreciated.

Associate editor: Brent T. Poe

References

Alberto, M.H.A.V., 1995. Structural characterization of $CaO–SiO_2–TiO_2–Fe–O$ glasses by Raman and Mössbauer spectroscopy. Ph.D., University of Coimbra.

Alberto, H.V., Gil, J.M., Ayres DeCampos, N., Mysen, B.O., 1993. Redox equilibria of iron in Ti-bearing calcium silicate quenched glasses. *J. Non-Cryst. Solids* **151**, 39–50.

Alberto, H.V., Pinto da Cunha, J.L., Mysen, B.O., Gil, J.M., de Campos, N.A., 1996. Analysis of Mössbauer spectra of silicate glasses using a two-dimensional Gaussian distribution of hyperfine parameters. *J. Non-Cryst. Solids* **194**, 48–57.

Bell, P.M., Mao, H.K., 1974. Crystal-field spectra of Fe^{2+} and Fe^{3+} in synthetic basalt glass as a function of oxygen fugacity. *Carnegie Instn. Wash. Year Book* **73**, 496–497.

Burkhard, D.J.M., 2000. Iron-bearing silicate glasses at ambient conditions. *J. Non-Cryst. Solids* **275**, 175–188.

Burns, R.G., 1994. Mineral Mössbauer spectroscopy: correlations between chemical shift and quadrupole splitting parameters. *Hyperfine Interact.* **91**, 739–745.

Calas, G., Petiau, J., 1983. Coordination state of iron in oxide glasses through high-resolution K-edge spectra: information from pre-edge. *Solid State Commun.* **48**, 625–629.

Dingwell, D.B., 1991. Redox viscometry of some Fe-bearing silicate melts. *Am. Mineral.* **76**, 1560–1562.

Dingwell, D.B., Virgo, D., 1987. The effect of oxidation state on the viscosity of melts in the system $Na_2O–FeO–Fe_2O_3–SiO_2$. *Geochim. Cosmochim. Acta* **51**, 195–205.

Dingwell, D.B., Webb, S.L., 1990. Relaxation in silicate melts. *Eur. J. Mineral.* **2**, 427–449.

Dyar, M.D., Naney, M.T., Swanson, S.E., 1987. Effect of quench methods on Fe^{3+}/Fe^{2+} ratios: a Mössbauer and wet-chemical study. *Am. Mineral.* **72**, 792–800.

Farges, F., Lefrere, Y., Rossano, S., Berthereau, A., Calas, G., Brown, G.E., 2004. The effect of redox state on the local structural environment

of iron in silicate glasses: a combined XAFS spectroscopy, molecular dynamics, and bond valence study. *J. Non-Cryst. Solids* **344**, 176–188.

Hannoyer, B., Lenglet, M., Durr, J., Cortes, J., 1992. Spectroscopic evidence of octahedral iron (III) in soda-lime-silicate glasses and crystals. *J. Non-Cryst. Solids* **151**, 109–216.

Henderson, G.S., Fleet, M.E., Bancroft, G.M., 1984. An X-ray scattering study of vitreous $KFeSi_3O_8$ and $NaFeSi_3O_8$ and reinvestigation of vitreous SiO_2 using quasicrystalline modelling. *J. Non-Cryst. Solids* **68**, 333–349.

Holland, D., Mekki, A., Gee, I.A., McConville, C.F., Johnson, J.A., Johnson, C.E., Appleyard, P., Thomas, M., 1999. The structure of sodium iron silicate glass—a multi-technique approach. *J. Non-Cryst. Solids* **253**, 192–202.

Jackson, W.E., Mustre de Leon, J., Brown, G.E., Waychunas, G.A., Conradson, S.D., Combes, J.-M., 1993. High-temperature XAS study of Fe_2SiO_4 liquid: reduced coordination of ferrous iron. *Science* **262**, 229–232.

Jackson, W.E., Farges, F., YEager, M., Mabrouk, P.A., Rossano, S., Waychunas, G.A., Solomon, E.I., Brown, G.E., 2005. Multispectroscopic study of Fe(II) in silicate glasses: implications for the coordination environment of Fe(II) in silicate melts. *Geochem. Cosmochim. Acta* **69**, 4315–4332.

Jayasuriya, K., O'Neill, H.S.C., Berry, A.J., Campbell, S.J., 2004. A Mössbauer study of the oxidation state of Fe in silicate melts. *Am. Mineral.* **89**, 1597–1609.

Keppler, H., 1992. Crystal field spectra and geochemistry of transition metal ions in silicate melts and glasses. *Am. mineral.* **77**, 62–75.

Kress, V.C., Carmichael, I.S.E., 1991. The compressibility of silicate liquids containing Fe_2O_3 and the effect of composition, temperature, oxygen fugacity and pressure on their redox states. *Contrib. Mineral. Petrol.* **108**, 82–92.

Lagarec, K., Rancourt, D.G., 1997. Extended Voigt-based analytical lineshape method for determining *N*-dimensional correlated hyperfine parameter distributions in Mössbauer spectroscopy. *Nucl. Instrum. Methods Phys. Res. Sect. B* **129**, 266–280.

Lange, R.A., Carmichael, I.S.E., 1989. Ferric–ferrous equilibria in Na_2O–FeO–Fe_2O_3–SiO_2 melts: effects of analytical techniques on derived partial molar volumes. *Geochim. Cosmochim. Acta* **53**, 2195–2204.

Larson, H., Chipman, J., 1953. Oxygen activity in iron oxide slags. *Trans. AIME* **196**, 1089–1096.

Matson, D.W., Sharma, S., Philpotts, J.A., 1986. Raman spectra of some tectosilicates and glasses along the orthoclase–anorthite and nepheline–anorthite joins. *Am. Mineral.* **71**, 694–704.

Mysen, B.O., Virgo, D., 1978. Influence of pressure, temperature, and bulk composition on melt structures in the system $NaAlSi_2O_6$–$NaFe^{3+}Si_2O_6$. *Am. J. Sci.* **278**, 1307–1322.

Mysen, B.O., Virgo, D., 1989. Redox equilibria, structure, and properties of Fe-bearing aluminosilicate melts: relationships between temperature, composition, and oxygen fugacity in the system Na_2O–Al_2O_3–SiO_2–Fe–O. *Am. Mineral.* **74**, 58–76.

Mysen, B.O., Dubinsky, E., 2004. Mineral/melt element partitioning and melt structure. *Geochim. Cosmochim. Acta* **68**, 1617–1634.

Mysen, B.O., Richet, P., 2005. *Silicate Glasses and Melts—Properties and Structure*. Elsevier, Amsterdam.

Mysen, B.O., Seifert, F., Virgo, D., 1980. Structure and redox equilibria of iron-bearing silicate melts. *Am. Mineral.* **65**, 867–884.

Mysen, B.O., Virgo, D., Seifert, F.A., 1984. Redox equilibria of iron in alkaline earth silicate melts: relationships between melt structure, oxygen fugacity, temperature and properties of iron-bearing silicate liquids. *Am. Mineral.* **69**, 834–848.

Mysen, B.O., Virgo, D., Neumann, E.R., Seifert, F.A., 1985a. Redox equilibria and the structural states of ferric and ferrous iron in melts in the system CaO–MgO–Al_2O_3–SiO_2: relations between redox equilibria, melt structure and liquidus phase equilibria. *Am. Mineral.* **70**, 317–322.

Mysen, B.O., Virgo, D., Scarfe, C.M., Cronin, D.J., 1985b. Viscosity and structure of iron- and aluminum-bearing calcium silicate melts. *Am. Mineral.* **70**, 487–498.

Mysen, B.O., Carmichael, I.S.E., Virgo, D., 1985c. A comparison of iron redox ratios in silicate glasses determined by wet-chemical and ^{57}Fe Mössbauer resonant absorption methods. *Contrib. Mineral. Petrol.*, 101–106.

Nagata, K., Hayashi, M., 2001. Structural relaxation of silicate melts containing iron oxide. *J. Non-Cryst. Solids* **282**, 1–6.

Neuville, D.R., Mysen, B.O., 1996. Role of aluminum in the silicate network: in-situ, high-temperature study of glasses and melts on the join SiO_2–$NaAlO_2$. *Geochim. Cosmochim. Acta* **60**, 1727–1738.

Neuville, D.R., Cormier, L., Massiot, D., 2004. Al environment in tectosilicate and peraluminous glasses: a ^{27}Al MQ-MAS NMR, Raman and XANES investigation. *Geochim. Cosmochim. Acta* **68**, 5071–5080.

Nolet, D.A., Burns, R.G., Flamm, S.L., Besancon, J.R., 1979. Spectra of Fe–Ti silicate glasses: implications to remote-sensing of planetary surfaces. In: *Proceedings of the 10th Lunar Planetary Science Conference*, pp. 1775–1786.

O'Horo, M.P., Levy, R.A., 1978. Effect of melt atmosphere on the magnetic properties of a $[(SiO_2)_{45}(CaO)_{55}]_{65}[Fe_2O_3]_{35}$ glass. *J. Appl. Phys.* **49**, 1635–1637.

Partzsch, G.M., Lattard, D., McCammon, C., 2004. Mössbauer spectroscopic determination of Fe^{3+}/Fe^{2+} in synthetic basalt glasses: a test of empirical f_{O2} equations under superliquidus and subliquidus conditions. *Conrib. Mineral. Petrol.* **147**, 565–580.

Paul, A., Douglas, R.W., 1965. Ferrous–ferric equilibrium in binary alkali silicate glasses. *Phys. Chem. Glasses* **6**, 207–211.

Presnall, D.C., Brenner, N.L., 1974. A method for studying iron silicate liquids under reducing conditions with negligible iron-loss. *Geochim. Cosmochim. Acta* **38**, 1785–1788.

Rossano, S., Behrens, H., Morin, G., Bauer, J.-P., Brouder, C., Calas, G., 1999. Study of iron oxidation state of tektites by Mössbauer effect. *Phys. Chem. Miner.* **26**, 530–538.

Rossano, S., Ramos, A.Y., Delaye, J.M., 2000. Environment of ferrous iron in $CaFeSi_2O_6$ glass: contributions of EXAFS and molecular dynamics. *J. Non-Cryst. Solids* **273**, 48–52.

Roy, B.N., Navrotsky, A., 1984. Thermochemistry of charge-coupled substitutions in silicate glasses: the systems $M_{1n}{}^{n+}AlO_2$–SiO_2 (M = Li, Na, K, Rb, Cs, Mg, Ca, Sr, Ba, Pb). *J. Am. Ceram. Soc.* **67**, 606–610.

Ryerson, F.J., 1985. Oxide solution mechanisms in silicate melts: systematic variations in the activity coefficient of SiO_2. *Geochim. Cosmochim. Acta* **49**, 637–651.

Spiering, B., Seifert, F.A., 1985. Iron in silicate glasses of granitic composition: a Mössbauer spectroscopic investigation. *Contrib. Mineral. Petrol.* **90**, 63–73.

Stebbins, J.F., Xue, X., 1997. NMR evidence for excess non-bridging oxygen in an aluminosilicate glass. *Nature (London)* **390**, 60–62.

Taylor, M., Brown, G.E., 1979. Structure of mineral glasses. II. The SiO_2–$NaAlSiO_4$ join. *Geochim. Cosmochim. Acta* **43**, 1467–1475.

Toplis, M.J., Kohn, S.C., Smith, M.E., Poplett, I.J.F., 2000. Fivefold-coordinated aluminum in tectosilicate glasses observed by triple quantum MAS NMR. *Am. Mineral.* **85**, 1556–1560.

Virgo, D., Mysen, B.O., 1985. The structural state of iron in oxidized vs. reduced glasses at 1 atm: a ^{57}Fe Mössbauer study. *Phys. Chem. Miner.* **12**, 65–76.

Wang, Z., Cooney, T.F., Sharma, S.K., 1993. High temperature structural investigation of $Na_2O \cdot 0.5Fe_2O_3 \cdot 3SiO_2$ and $Na_2O \cdot FeO \cdot 3SiO_2$ melts and glasses. *Contrib. Mineral. Petrol.* **115**, 112–122.

Waychunas, G.A., Brown, G.E., Ponader, C.W., Jackson, W.E., 1988. Evidence from X-ray absorption for network-forming Fe^{2+} in molten alkali silicates. *Nature* **332**, 251–253.

Wilke, M., Behrens, H., Burkhard, D.J.M., Rossano, S., 2002. The oxidation state of iron in silicic melt at 500 MPa water pressure. *Earth Planet. Sci. Lett.* **189**, 55–67.